

Exploring the Temporal Dynamics inside a Honeybee Colony

An ePortfolio

Course: Complex Systems, 800722-M-6

Professor: Travis Wiltshire

Academic year: 2024-2025, Spring semester

Submission date: 16-5-2025

Submission by Group 6

Group members and their executed tasks:

Djourdan Johnson: writing Module 10

Jacuqot Qiu: writing Module 4 and reviewing Module 10

Lotte Michels: finding a dataset and related literature, data exploration, writing Module 2, writing Module 7, writing DTW novelty aspect for Module 8, reviewing Module 6, reviewing Module 8, managing the Github repository, combining all work and handling submissions

Nawat Nawati Azhati: data exploration, writing Module 6, partly writing Module 12, reviewing Module 5 and reviewing Module 8

Nuo Xu: writing Module 5, partly writing Module 12 and reviewing Module 4

Xuelin Wei: writing Module 8 (without DTW)

Temporal Dynamics and Change

ePortfolio Entry 1 - Module 2

Group 6: Djourdan Johnson, Jacuqot Qiu, Lotte Michels, Nawat Nawati Azhati, Nuo Xu, Xuelin Wei

1 Introduction

For this Complex Systems project, we apply complexity science methods to investigate the dynamics of a beehive. We regard a beehive as a complex system, because it consists of many individual bees collectively producing complex behaviors, such as foraging, honey production, intrusion defense and temperature and humidity regulation. These behaviors emerge without any central control and dynamically change in response to environmental factors (Research and Consortium, 2010; Zhu et al., 2024).

The Multi-modal Sensor Dataset with Phenotypic trait measurements from honey Bees (MSPB) provides several longitudinal measurements in beehives (Zhu et al., 2024). In this first entry of our e-portfolio, various exploratory data techniques will be applied to create an initial understanding of the temporal dynamics within these data. Specifically, the various types of change, stationarity and stability within a singular beehive will be taken under the loop.

The code used for the computations and visualizations in this entry can be found [here](#).

2 MSPB Dataset Description

We will analyze parts of the Multi-modal Sensor Dataset with Phenotypic trait measurements from honey Bees (MSPB). Zhu et al. (2024) created this dataset by monitoring 53 beehives in Quebec between April 2020 and April 2021, collecting both longitudinal time-series data and phenotypic annotations.

The time-series consists of temperature, humidity and audio measurements. These signals were recorded every 15 minutes over one year of time. Temperature was measured inside the beehive chambers in degrees Celsius and humidity was measured inside the beehive chambers as a percentage. Moreover, audio recordings were automatically preprocessed to continuously compute the beehive ‘power’ of the hive. Conventionally, Zhu et al. (2024) use beehive power as a proxy for colony activity: a higher power score reflects a stronger buzzing, indicating an increase of bee presence in the hive. Hive power is measured in decibels (dB) and computed using the fast Fourier transform features covering frequencies between 122 Hz and 515 Hz. Please refer to the paper by Zhu et al. (2024) for an elaboration on the mathematical power formulas.

The phenotypic annotations are beehive characteristics that are sampled either once or a discontinuous and limited amount of times. The traits include number of brooding cells in

the hive, honey production, defense performance, hygiene performance and pesticide infestation level.

For this portfolio entry, we discuss and demonstrate complexity science analysis methods of temporal dynamics and patterns of change in the context of the MSPB dataset. We thus restrict ourselves to the time-series signals in the dataset (hive power, temperature and humidity) and investigate these for one single selected beehive: hive number 02204, located in the Coté apiary in Quebec.

3 Temporal Signatures

3.1 Types of Change in the MSPB Dataset

The behavior of a complex system over time is called its temporal pattern (Butner, 2018). A temporal pattern is not just the sum of the system’s constituents, rather it emerges from non-linear interactions between the individual time-series that occur within the system. Such time-series can display various types of change over time. Specifically, by means of visual exploratory inspection, a time-series can be assigned one of three temporal signatures (Butner, 2018):

1. **First-order change:** a signal shows constant, linear or curvilinear change over time.
2. **Second-order change:** a signal shows periodic behavior with a constant, changing or oscillating frequency component.
3. **Third-order change:** a signal shows chaotic and seemingly unpredictable behavior that heavily depends on the initial system conditions.

As a first step in the analysis of the MSPB time-series, we can explore which types of change are featured in the data. This dataset quickly reveals the scale-dependent nature of time-series: while temporal signatures may be obscured when viewing data over extended periods (e.g. multiple months), zooming in to shorter time spans (e.g. a week or a day) can uncover structures that are otherwise difficult to detect, or vice versa.

Figure 1 visualizes the scale-dependent nature of temporal structures. For example, plotted for the whole data collection period, the temperature signal shows third-order change: this signal features chaotic, non-linear and non-periodic change, with a trend downwards toward the end of the sequence. In contrast, the temperature plot for a randomly selected week within August reveals a clear second-order type of change:



Figure 1: Raw time-series from MSPB beehive nr. 02204 plotted over varying time series: temperature (top row), humidity (middle row) and activity (bottom row) with respect to the full measurement period (left column), one randomly selected week (middle column) and one randomly selected day within that week (right column).

the signal shows seven peaks and valleys, one for each day. This daily structure is even more defined in the plot made for a randomly selected day in the August week. The oscillatory structure from the weekly plot, however, is no longer observable in the daily temperature plot.

The humidity signal also shows a third-order temporal signature for the full data period: the plot shows chaotic, non-linear and non-periodic changes with varying trends over time. For the weekly plot, some sharp peaks and valleys may indicate an oscillatory trend, suggesting second-order change. Such peaks and valleys are visualized more clearly in the daily plot for humidity. However, focusing purely on this daily graph, one might argue that these peaks exhibit arbitrary trends and classify them as a third-order type of change.

Regarding the beehive activity/power signal, the full data plot appears very noisy and may reflect third-order change, but it could be argued that some global second-order trend is present: an overall oscillatory wave may be recognized, with a downwards trend towards the end of the data period. Zooming into one week of data reveals a more refined, but still noisy, oscillatory pattern. This indicates second-order change throughout a week in the data. Zooming into one day within this week, the power signal exhibits third-order change again. Zhu et al. (2024) explain that small fluctuations may occur in the power signal due to environmental noises

(like human speech, rain or wind) picked up by the audio recordings. This may explain why the power signal looks noisier than the humidity and temperature time-series.

Overall, the plots in Figure 1 - mostly those for the temperature signal - thus demonstrate the importance of exploring time-series on various time scales in order to confidently label them with the correct temporal signature. Depending on the research goal, some time scales may be more interesting than others. For our e-portfolio, we will analyze the full time-series within the MSPB dataset. This allows us to also explore seasonal honeybee behaviors (Research and Consortium, 2010), for instance when looking at pairwise coordination in entry 6. Keeping the scale-dependent nature of the beehive time-series in mind, we will regularly zoom in on smaller time periods within the data to account for local effects in our consecutive analysis.

3.2 Downsampling Effects

Time-series signals are sequences of measurements taken at a constant rate in time: the sampling rate. Choosing a suitable sampling rate is crucial to capture the actual temporal patterns within a signal (Butner, 2018). If sampling rate is too low, undersampling may occur. In this case, informative high-frequency dynamics are lost and the underlying temporal signature cannot be correctly identified. On the other hand, a

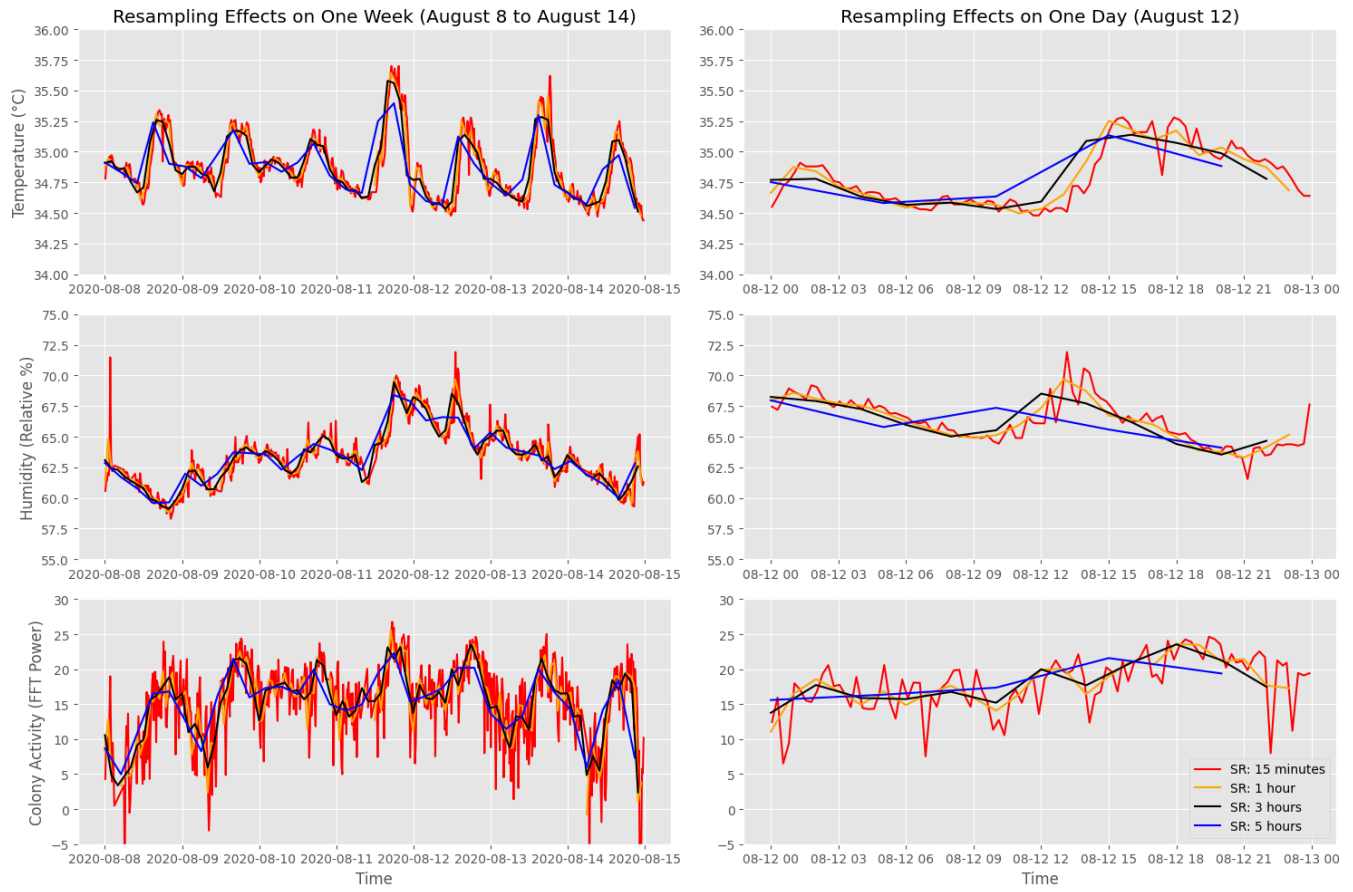


Figure 2: Sampling effects on the temperature, humidity and hive power signals of various sampling rates (SRs range between 15 minutes and 5 hours). For clarity, downsampling effects are displayed over the timecourses of one week (left) and one day (right).

very high sampling rate may lead to oversampling, in which case the proximity of measurements can make it difficult to detect patterns when the signal is plotted. In general, the higher the order of the temporal signature you hypothesize for your signal of interest, the more observations you want to make (Butner, 2018).

The time-series in the MSPB dataset are recorded every 15 minutes. Their values can be downsampled to check if the temporal signatures identified in these signals are susceptible to changes in sampling rate. Downsampling entails that the temporal resolution of a signal is reduced by grouping values into larger time intervals. For instance, 15 minute recordings can be converted to hourly averages. Downsampling is often applied to smooth out signal noise, but it can also lead to a loss of fine-grained trends in the signal.

We examined the downsampling effects for three different temporal resolutions: 1 hour, 3 hours and 5 hours. The results on the weekly and daily plots (which make resampling effects most clear) are displayed in Figure 2. These graphs show that down-sampling removes value variations within small time-scales, but puts more emphasis on the global signal trends. Whereas the order and complexity of the signal attenuate in the daily plots with decreasing temporal resolution, the temporal signatures and trends remain mostly identifiable in the weekly plots.

4 Time-Series Stability

4.1 Stability of Signal Values

To further investigate change, we can look at the distribution of the values and residuals in a time-series. Histograms or density plots (smoothed histograms) of raw values give an indication of the stable values that a signal is centered around, which will form peaks in the plot (Butner, 2018). These values represent the states that a signal tends to center around. The narrower a density plot is around a peak, the closer the signal stays to this value. Conversely, the wider a density plot is, the more the signal tends to deviate from this central value. Density plots can show more than one peak, in which case the signal features multiple stable states: this is called multistability. Alternatively, if a density plot shows no notable peaks, this may indicate an unstable temporal course of the signal (lack of stable states).

The density plots for the raw temperature, humidity and power signal values are displayed in the top row of Figure 3. For all three signals, these plots indicate multistability. The temperature plot shows a sharp peak around 35 degrees celcius. This peak makes sense in the context of typical beehive phenomena: thermoregulation, a well-known emergent honeybee colony characteristic, keeps the beehive temperature more or less constant between 33 to 38 degrees (Research and

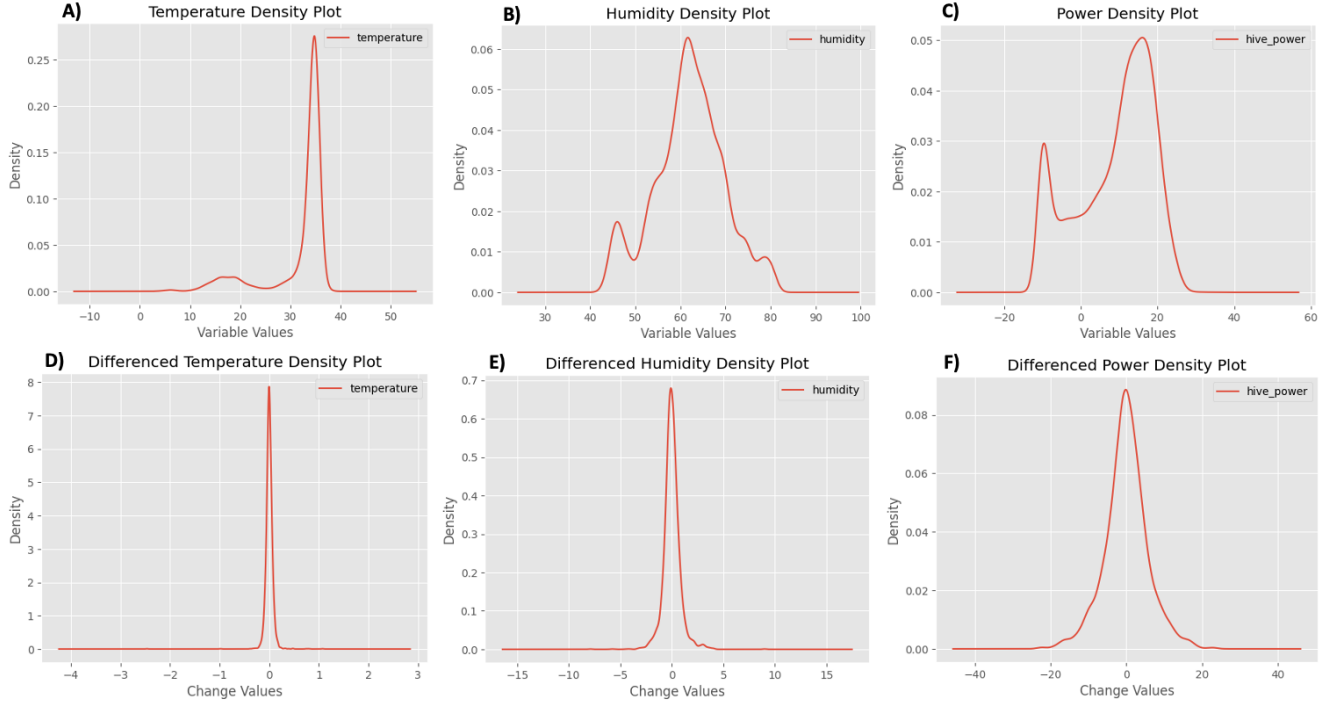


Figure 3: Density plots visualizing the stability of temporal signals and their change. A-C: density plots of the raw temperature, humidity and power values. D-F: density plots of the residuals within the respective signals.

Consortium, 2010). Effectively controlling this temperature level has been found to increase honey production and brood development and decrease bee mortality rates (Research and Consortium, 2010; Zhu et al., 2024). Similarly, the optimum levels for beehive humidity have been found to lie between 50% and 60% (Zhu et al., 2024). This is also reflected in the main peak in plot B in Figure 3.

Both the temperature and humidity density plots also show smaller peaks, around 18 degrees celsius and 45% and 80% respectively. It appears that these smaller peaks are created by sudden signal fluctuations at the end of the measurement period, as visible in Figure 1. According to Zhu et al. (2024), such sudden fluctuations regarding internal beehive temperature and humidity may reflect the presence of an active queen bee or the occurrence of honeybee swarming behavior.

For the beehive power, the density plot in Figure 3 also indicates two stable states. Most of the signal values are centered around a power value of 18 dB. The plot features an additional peak around -10 dB, which seems to be the cutoff of the power computation (Zhu et al., 2024).

4.1.1 Measurement Errors Effects

In addition to his notions of temporal patterns, Butner (2018) described three notions of variability in a signal:

1. **Perturbations:** disturbances that cause a system to deviate from its stable state(s).
2. **Random Walk:** cumulative noise that causes a drift in the signal trend.
3. **Measurement Error (ME):** imprecisions in signal recordings, possibly introducing biases in the data.

Contrary to the first two notions, ME can change the 'real values' in a sequence and thus affect the signal stability. To assess how susceptible a system is to ME, various degrees of random noise can be added to explore the effects on the system's stable states.

We examined ME effects on the beehive temperature, humidity and power signals by adding random noise with increasing standard deviation units to the time-series, and plotting the resulting density curves against each other. These curves are displayed in Figure 4. For all three signals, the graphs show that the most prominent peaks in the density plots remain, but are flattened for large standard deviation settings. Moreover, the smaller peaks in the original multi-stability density plots quickly attenuate as ME noise is added. This attenuation is most prominent for the -10 dB peak in the power density plot, suggesting this peak may be a bias in the data created by measurement error. Zhu et al. (2024) also described the power signal to be most sensitive to such noise, as the audio recordings used to compute the power signal may pick up on environmental sounds.

4.2 Stability of Change

In addition to the raw signal density plots, we can create similar graphs for the sequence residuals to get an idea of the stability of temporal *change* in a time-series. That is, we compute the differences between consecutive values in a signal and plot these to investigate the distribution of signal fluctuations. If a residual density plot is centered around zero, this suggests mean signal stability. Moreover, a narrow distribution/density plot indicates consistently small value changes between consecutive timesteps, which may suggest signal sta-

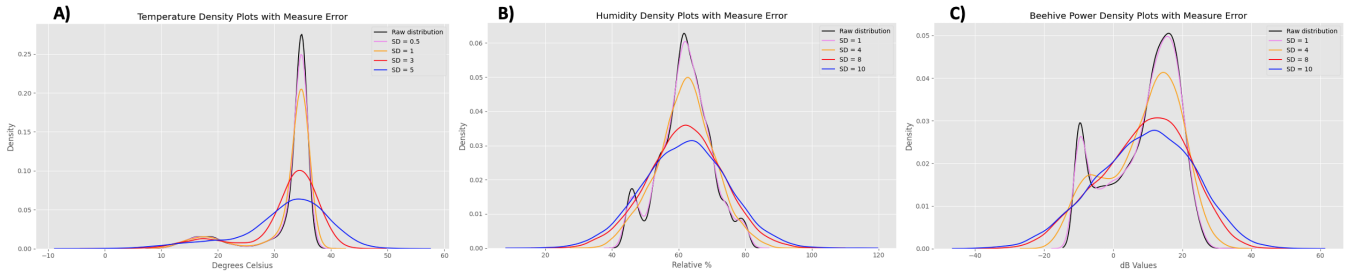


Figure 4: Density plots visualizing signal stability under varying degrees of random noise. For temperature (A), noise standard deviations range from 0.5 to 5. For humidity and power (B and C), noise standard deviations range from 0.5 to 10.

tionarity. On the other hand, flat and spread-out plots display large and variable differences over time and may suggest signal non-stationarity. Lastly, asymmetry in residual density plots may indicate an up- or downwards trend in the signal (for left- or right-skewed distributions respectively). However, it is important to note that conclusions about signal trend and stationarity should be supported and mostly drawn from visual inspection and statistical tests.

The density plots for the residual temperature, humidity and power signal values are displayed in Figure 3. All these residual plots are centered around zero, which indicates that all signals are stable around their means: 31.8 (sd: 6.2), 62.0 (sd: 7.8) and 8.7 (sd: 10.0) respectively. Matching the standard deviation statistics, the residual density plot is most narrow for temperature, followed by humidity and lastly by the power residuals. Similarly, value differences between consecutive measurements are smallest for temperature, followed by humidity and lastly by the power signal.

Based on the analysis displayed in Figure 3, we can thus infer that out of the three time-series, the temperature signal is most stable and the power signal is most unstable. As explained, the narrow density plots may indicate signal stationarity. However, more fine-grained analyses are necessary to draw such conclusions. We will therefore look at stationarity tests in the next section.

5 Statistical Stationarity Analysis

So far we have inspected the dynamics in MSPB time-series with regards to their types of change and stability. The residual density plots from the previous section suggested that the temperature, humidity and power signals may be stationary over time. Stationarity in a sequence entails that the dynamics in a signal do not change over time (Butner, 2018). It is important to assess stationarity in a signal, as some complexity science analyses may make the assumption that signal dynamics remain stable over time. An example would be the Granger causality test, covered in entry 8 (Module 12) of our e-portfolio.

To empirically assess whether a time-series is stationary, statistical tests can be conducted. Conventionally, we will apply and compare two such methods: the Augmented Dickey-Fuller (ADF) test and the Kwiatkowski-Phillips-Schmidt-Shin (KPSS) test (Dickey and Fuller, 1979; Kwiatkowski et al., 1992).

While they both check for data stationarity, the ADF and

Signal	ADF		KPSS	
	Test (statistic)	P-value	Test (statistic)	P-value
Temperature	False (-1.9)	0.35	False (3.17)	< 0.01
Humidity	True (-3.2)	0.02	False (2.6)	< 0.01
Power	True (-4.2)	< 0.01	True (0.4)	0.08

Table 1: ADF and KPSS test results for the stationarity within the MSPB time-series in beehive 02204. Contradicting test results are highlighted in bold text.

KPSS tests have opposite null hypotheses: The ADF test's null hypothesis is that the time series has a unit root (i.e., it is non-stationary), while the KPSS test's null hypothesis is that the series is stationary. So, for the ADF test, a significant test statistic or low p-value suggests the signal is stationary, whereas for the KPSS test, a significant test statistic or low p-value suggests the signal is not stationary. They can be used complementarily to cross-validate conclusions about stationarity. Such cross-validation is important, as the tests may sometimes give contradicting outputs due to slightly different computational sensitivities. This is also demonstrated by Table 1.

Table 1 summarizes the ADF and KPSS test results for the beehive time-series. The dynamics in the beehive power signal appear to be stationary over time. In contrast, both tests classify the temperature signal as non-stationary throughout the measurement period. This finding matches with the signal's visualization in Figure 1. Regarding the humidity signal, the test results are inconclusive. Looking at the signal's plot in Figure 1, we argue the sequence looks some-what non-stationary. As such, we will not assume stationarity for the humidity signal.

6 Conclusion

In this first e-portfolio entry, we introduced the topic of our project and provided a description of the dataset that will be analyzed. Moreover, a variety of exploratory data techniques was applied to get a better idea of the temporal signals (temperature, humidity and colony activity (power)) that will

be further taken under the loop in the upcoming e-portfolio entries.

It was found that all time-series display third-order change over the full measurement period, while some second-order oscillatory patterns may be identified by zooming in to a smaller time-scale. Moreover, high resistance to downsampling effects was found for these temporal signatures. Next, it was observed that all time-series tended towards multistability in their signal values. However, an analysis of measurement error effects indicated that this multistability dissipates quickly under randomly added Gaussian noise. In addition, all signals showed zero-centered uni-stability in their residuals, suggesting signal stationarity. However, ADF and KPSS stationarity tests indicated only the beehive power signal to be stationary over time.

References

- [Butner2018] Jon Butner. 2018. *Quantitative Reasoning Under a Dynamical Social Science*. University of Utah, 1.02 edition, 6.
- [Dickey and Fuller1979] David A. Dickey and Wayne A. Fuller. 1979. Distribution of the Estimators for Autoregressive Time Series with a Unit Root. *Journal of the American Statistical Association*, 74(366a):427–431, 6.
- [Kwiatkowski et al.1992] Denis Kwiatkowski, Peter C.B. Phillips, Peter Schmidt, and Yongcheol Shin. 1992. Testing the null hypothesis of stationarity against the alternative of a unit root. *Journal of Econometrics*, 54(1-3):159–178, 10.
- [Research and Consortium2010] Mid-Atlantic Apiculture Research and Extension Consortium. 2010. Seasonal Cycles of Activities in Colonies, 6.
- [Zhu et al.2024] Yi Zhu, Mahsa Abdollahi, Ségolène Maucourt, Nico Coallier, Heitor R. Guimarães, Pierre Giovenazzo, and Tiago H. Falk. 2024. MSPB: a longitudinal multi-sensor dataset with phenotypic trait measurements from honey bees. *Scientific Data*, 11(1), 8.

Attractor Dynamics Analysis of Beehive Data from MSPB Dataset

ePortfolio Entry 2 - Module 4

Group 6: Djourdan Johnson, Jacuqot Qiu, Lotte Michels, Nawat Nawati Azhati, Nuo Xu, Xuelin Wei

Abstract

This report analyzes the environmental regulation behavior of a honeybee colony (tag number 202204) based on sensor data from the MSPB dataset (Multi-Sensor dataset with Phenotypic trait measurements from honey Bees). Applying attractor dynamics theory through state space reconstruction, phase portraits, vector field analysis, and topological mapping, we reveal the dynamic characteristics, stable patterns, and self-organizing behavior of the beehive system. Results indicate that the bee colony demonstrates strong environmental self-regulation capabilities, exhibiting clear attractor structures in temperature and humidity dimensions.

Keywords: Attractor Dynamic

1 Introduction

Honeybee colonies, as complex biological systems, maintain stable internal hive environments through collective behavior. This study employs methods from nonlinear dynamics, specifically attractor dynamics, to characterize and analyze the dynamic interplay between temperature and humidity within honeybee hives(Khoury et al., 2011). The concept of attractors provides a framework for understanding system stable states, helping to reveal how bee colonies respond to environmental disturbances and maintain suitable conditions.

The data analyzed in this study comes from the MSPB dataset (Zhu et al., 2023), a comprehensive one-year longitudinal dataset collected between April 2020 and April 2021 from 53 hives in two apiaries in Québec, Canada. This dataset uniquely combines continuous sensor data (including temperature, humidity, and audio features) with expert-annotated phenotypic measurements such as hive population, brood cells, Varroa destructor infestation levels, defensive and hygienic behaviors, honey yield, and winter mortality. Our analysis focuses specifically on beehive 202204, examining the temperature-humidity dynamics from the perspective of attractor theory. The thesis code can be accessed through the GitHub repository at [code link](#).

2 Data and Methods

2.1 Dataset Description

The analysis is based on sensor data from the MSPB dataset (Multi-Sensor dataset with Phenotypic trait measurements from honey Bees), which includes the following key variables:

Table 1: Beehive Monitoring Variables

Variable	Description
published_at	Timestamp
temperature	Temperature
humidity	Humidity
tag_number	Beehive identification (analysis limited to beehive 202204)
hive_power	Hive power
geolocation	Geographic location information
hz_*	Multiple frequency variables

Beehive 202204 was specifically selected for this analysis because it contains the most complete and usable data within the MSPB dataset, particularly during the summer months of July and August. With approximately 4,000 measurement points per month (Zhu et al., 2023), this beehive provides a robust dataset for analyzing environmental dynamics. The high temporal resolution of the measurements allows for detailed characterization of the temperature-humidity state space and attractor patterns.

While the MSPB dataset also contains rich phenotypic measurements including beehive population, brood cell counts, Varroa mite infestation levels, defensive and hygienic behaviors, honey yield, and winter mortality, our current analysis focuses exclusively on the sensor data related to temperature and humidity dynamics. The data was collected as part of a comprehensive study conducted between April 2020 and April 2021 across 53 hives in Québec, Canada.

2.2 Analytical Methods

This study employs the following dynamical analysis methods:

- **State Space Reconstruction:** Using temperature and humidity as primary state variables to construct a two-dimensional state space (Deyle and Sugihara, 2011)
- **Phase Portrait Analysis:** Visualizing system trajectories by calculating velocity vectors to identify stable and unstable regions (Eckmann et al., 1987)
- **Vector Field Analysis:** Computing velocity vectors on a state space grid to demonstrate system evolution trends at different state points (Letellier et al., 1995)
- **Topological Mapping (Density Analysis):** Using kernel density estimation to identify frequently visited regions in state space (attractors)(Deyle and Sugihara, 2011)

- **Regression Analysis:** Building regression models to predict state changes and quantify system feedback mechanisms

3 Results Analysis

3.1 State Space Reconstruction

The state space plot (Fig. 1) provides a direct visualization of the system's trajectory in temperature-humidity coordinates without calculating velocity vectors. A strong inverse relationship between temperature and humidity is evident across most of the state space, appearing as a diagonal trend from the upper left (low temperature, high humidity) to the lower right (high temperature, low humidity). The majority of trajectories follow this diagonal pattern, suggesting a fundamental thermodynamic relationship in the beehive environment. Significant clustering and dense trajectory patterns appear in two main regions: around $32\text{--}35^\circ\text{C}$ with $45\text{--}65\%$ humidity and around $5\text{--}10^\circ\text{C}$ with $75\text{--}80\%$ humidity. The trajectories show increased complexity and non-linear patterns at the higher temperature range ($30\text{--}35^\circ\text{C}$), with circular and looping patterns suggesting active regulation by the bee colony. Some outlier trajectories deviate from the main diagonal trend, potentially indicating periods of transition or disturbance in the hive environment. This state space reconstruction forms the foundation for the subsequent dynamical analyses and clearly demonstrates that the beehive system does not behave as a simple linear system, but exhibits complex, regulated patterns with preferred regions in the state space.

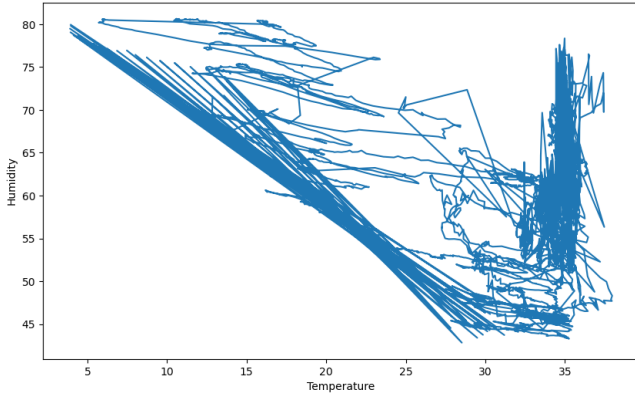


Figure 1: State space plot of temperature-humidity system

3.2 Phase Space Analysis

The phase portrait (Figure 2) displays the trajectories and velocity vectors of the temperature-humidity system. Observations indicate that the system exhibits distinct directional flow, particularly in high-temperature regions ($30\text{--}35^\circ\text{C}$). Vector directions indicate multiple convergence zones, suggesting the system has stabilizing tendencies at specific state combinations. Temperature and humidity demonstrate complex non-linear relationships, with different interaction patterns across different regions. Higher vector density in high-temperature regions ($> 30^\circ\text{C}$) indicates more frequent regulation behavior by the bee colony in this temperature range.

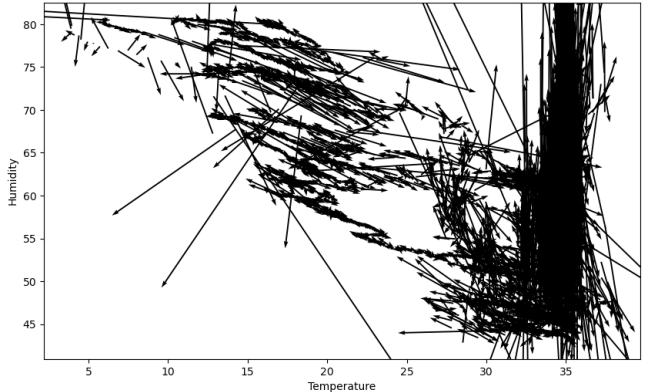


Figure 2: Phase Portrait of Beehive Dynamics

3.3 Vector Field Analysis

The vector field plot (Figure 3) provides a macroscopic view of the system's overall flow tendencies. It clearly shows that the system's primary flow direction converges toward the upper right region ($30\text{--}33^\circ\text{C}$, $60\text{--}65\%$ humidity). Distinct boundaries exist in the flow field, indicating different dynamical behaviors in different regions. Vector strength (arrow length) varies significantly across regions, suggesting different response intensities to deviations from different stable states. Vectors from peripheral regions (such as high-temperature, low-humidity areas) point toward the main attractor region, indicating the system's tendency to return to typical stable states.

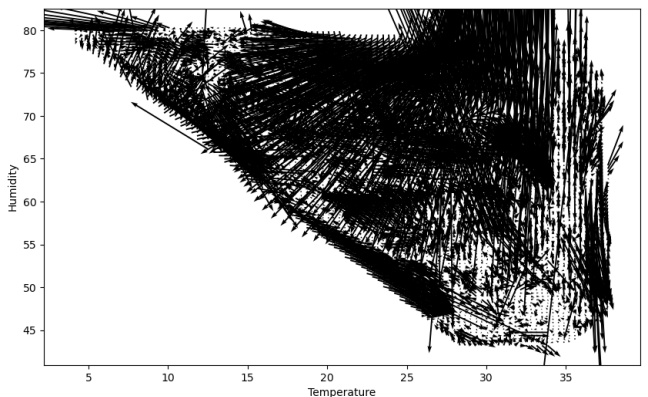


Figure 3: Vector Field of Beehive Dynamics

3.4 Topological Analysis

The topology plot (Figure 4) reveals the probability distribution of the state space through density contours. Two distinct high-density regions (attractors) exist: a primary attractor centered at $32\text{--}33^\circ\text{C}$ and $60\text{--}62\%$ humidity, with density values up to 0.018, and a secondary attractor located at $33\text{--}34^\circ\text{C}$ and $45\text{--}47\%$ humidity, with density values around 0.003. Attractors exhibit elliptical shapes with the major axis along the diagonal, indicating correlation between temperature and humidity changes. The primary attractor's area and density are significantly greater than the secondary attractor, suggest-

ing the system preferentially operates in this state. The low-density region between the two attractors suggests potential transition mechanisms between these two stable states.

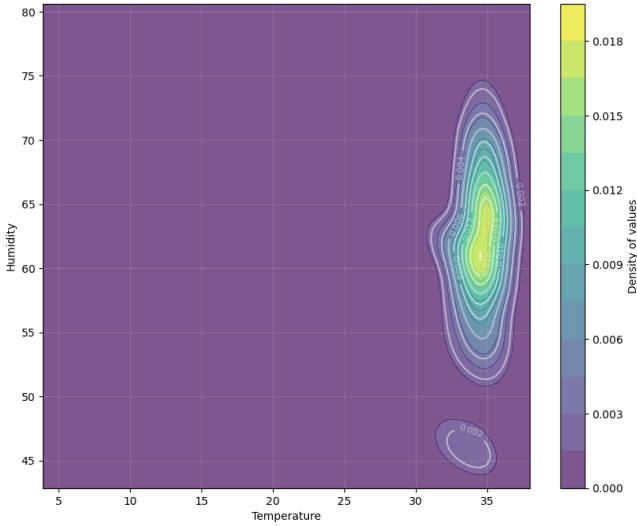


Figure 4: 2D Topology Piloy - Temperature vs. Humidity

3.5 Regression Analysis

The analysis aimed to quantify the influence of current states (temperature and humidity) on future system changes (temperature and humidity changes). The model was developed using a **Vector Autoregressive (VAR)** approach, which is suitable for capturing the dynamic interdependencies between the variables over time. The VAR model estimates how past values of temperature, humidity, and their changes affect future values of these variables. While the model captures significant relationships, the overall explanatory power of individual equations is limited, with relatively low R-squared values for each equation. The VAR results are presented in Table 2.

3.5.1 Model Specification

The VAR model includes the following system of equations, where the temperature change, humidity change, and their lags are used as predictors:

$$\begin{aligned} \Delta T_{t+1} &= \beta_0 + \beta_1 \cdot T_t + \beta_2 \cdot H_t + \dots + \epsilon_t \\ \Delta H_{t+1} &= \gamma_0 + \gamma_1 \cdot T_t + \gamma_2 \cdot H_t + \dots + \epsilon_t \end{aligned} \quad (1)$$

Where:

- ΔT_{t+1} is the change in temperature at time $t + 1$,
- ΔH_{t+1} is the change in humidity at time $t + 1$,
- T_t and H_t are the current temperature and humidity,
- The ellipsis (\dots) represents the lagged variables (e.g., previous time steps for temperature and humidity).

3.5.2 Model Results

The VAR regression results for temperature and humidity changes are summarized in Table 2. The results include the coefficients, standard errors, t-statistics, and p-values for each variable and lag, as well as the model's overall fit statistics.

Table 2: VAR Regression Results (N=12,429)

Statistic	Value
R-squared (Temperature)	0.021
R-squared (Humidity)	0.019
F-statistic (Temperature)	131.1
F-statistic (Humidity)	119.8
Prob (F-statistic)	4.38e-57
Coefficients (Temperature)	0.0161
Coefficients (Humidity)	-0.0331
Condition Number	821

3.5.3 Diagnostic Analysis

Three primary issues were identified: (1) Multicollinearity between predictors, as indicated by some NaN values in the standard errors of lagged coefficients, particularly for temperature and humidity, suggesting that these variables may be highly correlated, (2) Inherent nonlinear dynamics suggested by the system's residuals and the potential instability of some lagged coefficients, which may require further investigation using nonlinear modeling techniques, and (3) the large sample size (N=12,429), which may have contributed to amplifying these computational challenges.

4 Discussion

4.1 Bee Colony Environmental Regulation Mechanisms

The analysis results reveal the efficient environmental regulation capabilities of the bee colony. The presence of the primary attractor (32-33 °C, 60-62% humidity) indicates that the colony actively maintains these specific environmental conditions, which align with the optimal temperature range for brood development (33-36 °C)(Mucci et al., 2021). The strong tendency of the system toward the primary attractor suggests that collective colony behavior effectively resists external environmental fluctuations. The existence of a secondary attractor may reflect alternative stable states under different physiological demands or external conditions.

4.2 Dynamical Characteristics and Biological Significance

The state space reconstruction (Image 4) reveals the fundamental temperature-humidity relationship throughout the beehive's operational range, showing both the broad thermodynamic constraints and the regions where active regulation occurs. The dual attractor structure suggests the colony may have two operational "modes," with the primary mode focused on brood environment maintenance and the secondary mode potentially related to other functions (such as honey storage, ventilation). The temperature-humidity inverse correlation likely reflects the behavioral strategy of increasing ventilation to reduce humidity under high-temperature conditions(Rodríguez-Vásquez et al., 2024). The consistency of the vector field indicates strong buffering capacity against environmental disturbances, which is crucial for maintaining colony stability.

4.3 Methodological Limitations

The current analysis has several limitations. Only temperature and humidity variables were considered, while the actual system may be influenced by multiple factors. The analysis does not fully account for the impact of daily cycles and seasonal variations on the system. Linear regression cannot capture the complex nonlinear dynamic characteristics of the system. Additionally, observational data cannot determine the causal direction of temperature-humidity changes (whether bee colony behavior causes or responds to environmental changes) (Yuan and Shou, 2022).

5 Conclusion

The beehive system exhibits clear attractor dynamics characteristics, forming stable states primarily in the region of 32-33 °C and 60-62% humidity. The system contains a secondary attractor (33-34 °C, 45-47% humidity), suggesting the colony may have multiple operational modes. Vector field and phase space analysis indicate that the bee colony possesses strong environmental regulation capabilities, actively pulling the system back to stable states. The complex relationship between temperature and humidity suggests that the colony's environmental regulation is a highly coordinated process(Stabentheiner et al., 2010).

References

- [Yuan and Shou2022] Alex Eric Yuan and Wenying Shou. 2022. Data-driven causal analysis of observational biological time series. *eLife*, 11:e72518, aug.
- [Zhu et al.2023] Yi Zhu, Mahsa Abdollahi, Ségolène Maucourt, Nico Coallier, Heitor R. Guimarães, Pierre Giovenazzo, and Tiago H. Falk. 2023. Mspb: a longitudinal multi-sensor dataset with phenotypic trait measurements from honey bees.
- [Deyle and Sugihara2011] Ethan R. Deyle and George Sugihara. 2011. Generalized theorems for nonlinear state space reconstruction. *PLOS ONE*, 6(3):1–8, 03.
- [Eckmann et al.1987] J.-P. Eckmann, S. Oliffson Kamphorst, and D. Ruelle. 1987. Recurrence plots of dynamical systems. *Europhysics Letters*, 4(9):973, nov.
- [Khoury et al.2011] David S. Khoury, Mary R. Myerscough, and Andrew B. Barron. 2011. A quantitative model of honey bee colony population dynamics. *PLoS ONE*, 6(4):e18491, April.
- [Letellier et al.1995] C. Letellier, L. Le Sceller, E. Maréchal, P. Dutertre, B. Maheu, G. Gouesbet, Z. Fei, and J. L. Hudson. 1995. Global vector field reconstruction from a chaotic experimental signal in copper electrodissolution. *Phys. Rev. E Stat. Phys. Plasmas Fluids Relat. Interdiscip. Topics*, 51(5):4262–4266, May.
- [Mucci et al.2021] Claudio Andoni Mucci, Leonor Ramirez, Rocío Soledad Giffoni, and Lorenzo Lamattina. 2021. Cold stress induces specific antioxidant responses in honey bee brood. *52(3):596–607*.
- [Rodríguez-Vásquez et al.2024] Samantha Rodríguez-Vásquez, Alfonso Gardea, Alejandro Romo, Jaqueline García-Hernández, Humberto Ríos, and Jesús Orozco-Avitia. 2024. Hive temperature regulation by honeybees in response to extreme conditions. *Agrociencia*, 05.
- [Stabentheiner et al.2010] Anton Stabentheiner, Helmut Kovac, and Robert Brodschneider. 2010. Honeybee colony thermoregulation-regulatory mechanisms and contribution of individuals in dependence on age, location and thermal stress. *PLoS One*, 5(1):e8967.

Phase Space Reconstruction Analysis Report for Beehive Dynamics

Entry 3 - Module 5

Group 6: Djourdan Johnson, Jacuqot Qiu, Lotte Michels,
Nawat Nawati Azhati, Nuo Xu, Xuelin Wei

Abstract

This report presents the phase space reconstruction analysis of three variables—temperature, humidity, and hive power—from beehive sensor data (tag number 202204, July–August 2020). The analysis follows the methodology of Module 5, focusing on single-variable phase space reconstruction to understand the dynamics of each variable. We explore the deterministic and periodic nature of these variables using Takens' Delay Embedding Theorem (Takens, 1981), correlation dimension estimation, and surrogate data methods.

1 Introduction

Understanding the dynamics of beehive environmental variables is crucial for monitoring hive health. This study applies phase space reconstruction to three time series—temperature, humidity, and hive power—from a beehive sensor dataset (tag number 202204, July–August 2020). Following Module 5, we use single-variable phase space reconstruction to investigate the deterministic and periodic nature of these variables. The analysis employs Takens' Delay Embedding Theorem (Takens, 1981) to reconstruct the phase space, estimates correlation dimensions to assess dynamic complexity, and uses surrogate data to evaluate result robustness (Module 7: Surrogate Methods).

2 Methods

We applied single-variable phase space reconstruction to each variable using the following steps:

- **Data Preprocessing:** Removed duplicate timestamps, subsampled every 8th point to reduce computational load, and retained original trends without detrending.
- **Exploratory Visualization:** Plotted time series, pairwise scatter plots, and a 3D vector field with density to observe trends and relationships.
- **Phase Space Reconstruction:** Used Takens' Delay Embedding Theorem (Takens, 1981) to reconstruct the phase space with the `buildTakens` function.
- **Parameter Selection:** Initially estimated time delay (τ) using Average Mutual Information (AMI) and embedding dimension (M) with Cao's method (Cao, 1997), then optimized via sensitivity analysis.

- **Correlation Dimension:** Calculated the correlation dimension to quantify dynamic complexity.
- **Surrogate Data:** Generated surrogate data to test robustness (Module 7: Surrogate Methods). A significantly lower original dimension compared to the surrogate indicates deterministic dynamics.
- **Visualization:** Generated phase space plots to visualize trajectories.

3 Results

3.1 Data Overview and Preprocessing

We analyzed three time series from the beehive sensor data:

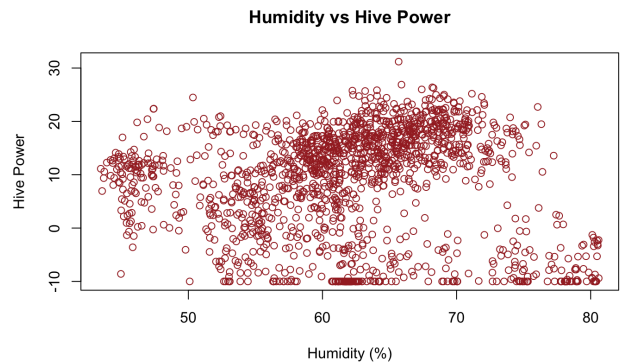
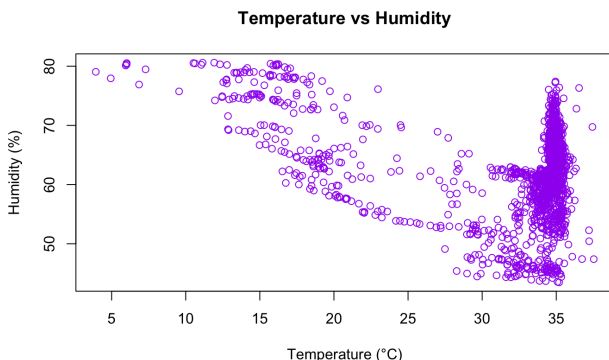
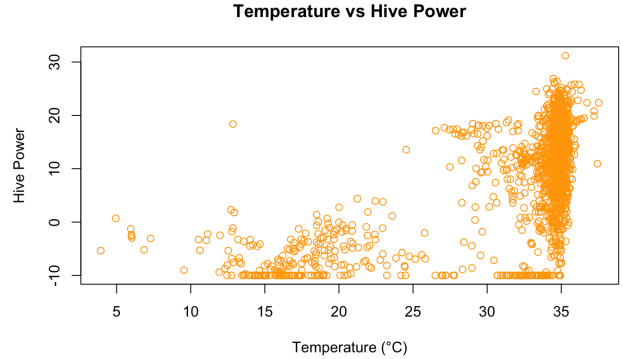
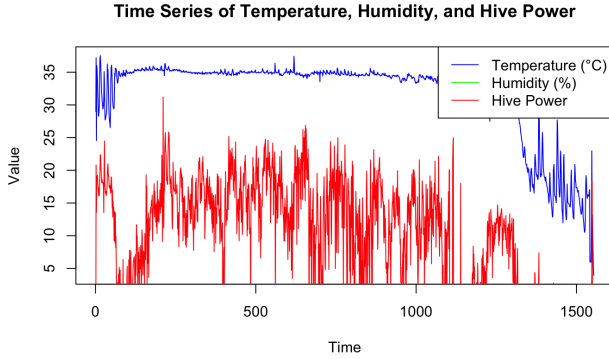
- **Temperature:** Range 3.93°C to 37.53°C, mean 31.80°C, standard deviation 6.31233.
- **Humidity:** Range 43.47% to 80.60%, mean 62.04%, standard deviation 7.836648.
- **Hive Power:** Range -10.000 to 31.197, mean 8.732, standard deviation 10.05023.

Preprocessing:

- Removed duplicate timestamps based on `published_at`.
- Subsampled the data by taking every 8th point (reducing from ~8000 to ~1000 points) to lower computational load, retaining main dynamic features.
- Did not detrend the data to preserve long-term dynamics (e.g., daily cycles).

Exploratory Visualization:

- **Time Series Plot:** Showed possible daily cycles in temperature and humidity, with hive power exhibiting burst-like variability (Figure 1).
- **Pairwise Scatter Plots:** Revealed an inverse relationship between temperature and humidity, and variable patterns in hive power (Figures 2, 3, and 4).
- **Vector Field and Density Plot:** Visualized dynamic flow in 3D, using change rates as a density proxy (Figure 5).



3.2 Phase Space Reconstruction

Initial parameter estimation used AMI for τ and Cao's method for M :

- Temperature: $\tau = 38, M = 8$, Correlation Dimension = 3.198562 (Surrogate = 3.725026).
- Humidity: $\tau = 13, M = 9$, Correlation Dimension = 7.530213 (Surrogate = 3.695639).
- Hive Power: $\tau = 1, M = 3$, Correlation Dimension = 1.309729 (Surrogate = 2.698470).

Sensitivity analysis tested τ (2, 4, 6, 8) and M (2, 4, 6):

- Temperature: Dimensions ranged from 1.015674 to 2.377713 (surrogate: 1.256028 to 3.771640), lower at smaller τ and M (Figures 6 and 7).
- Humidity: Dimensions ranged from 1.866193 to 5.684184 (surrogate: 1.968508 to 5.870703), often higher than surrogate at larger M , suggesting noise (Figures 8 and 9).
- Hive Power: Dimensions ranged from 1.384295 to 5.404614 (surrogate: 1.710832 to 5.417492), lower at

smaller τ and M , indicating deterministic dynamics (Figures 10 and 11).

Optimized parameters were selected where the correlation dimension was lowest and significantly below the surrogate:

- Temperature: $\tau = 2, M = 6$
- Humidity: $\tau = 2, M = 2$
- Hive Power: $\tau = 2, M = 2$

Final results with optimized parameters:

- **Temperature:** Dimensions: 1544×6 . Correlation Dimension: 1.995383 (Surrogate: 3.718860). Deterministic dynamics confirmed (Figure 12).
- **Humidity:** Dimensions: 1552×2 . Correlation Dimension: 1.866193 (Surrogate: 1.978875). Small difference suggests possible noise (Figure 13).
- **Hive Power:** Dimensions: 1552×2 . Correlation Dimension: 1.384295 (Surrogate: 1.717435). Deterministic dynamics with possible periodicity (Figure 14).

Hive Power Periodicity Attempt: Tested $\tau = 360, M = 3$, but the plot showed irregular lines rather than a closed loop (Figure 15).

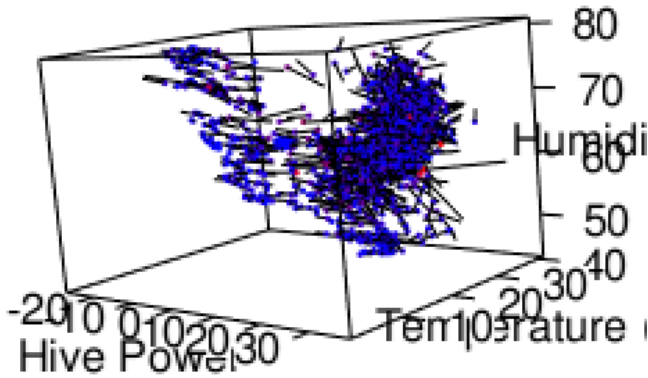


Figure 5: Vector Field and Density Plot (Temperature vs. Humidity vs. Hive Power)

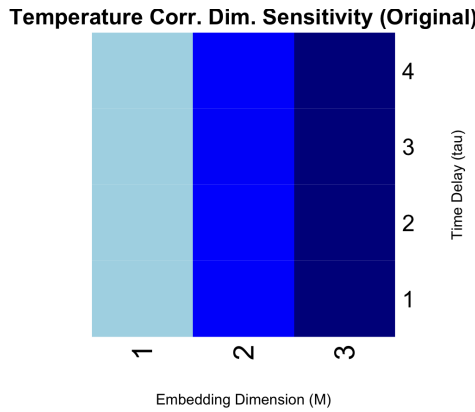


Figure 6: Sensitivity Analysis Heatmap for Temperature (Original)

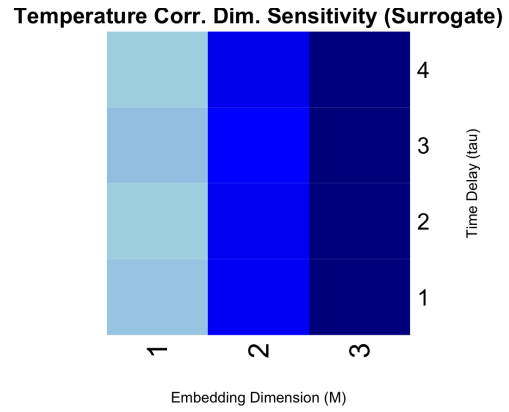


Figure 7: Sensitivity Analysis Heatmap for Temperature (Surrogate)

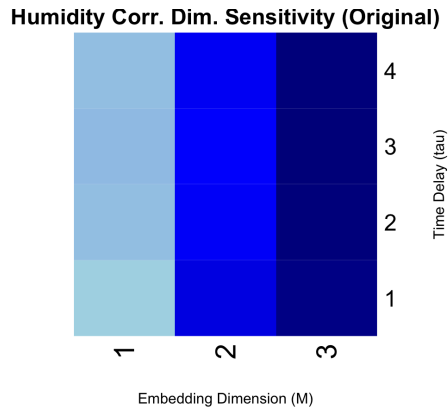


Figure 8: Sensitivity Analysis Heatmap for Humidity (Original)

References

- Takens, F. (1981). Detecting strange attractors in turbulence. In *Dynamical Systems and Turbulence, Warwick 1980* (pp. 366–381). Springer.
- Cao, L. (1997). Practical method for determining the minimum embedding dimension of a scalar time series. *Physica D: Nonlinear Phenomena*, 110(1-2), 43–50.

4 Discussion

Temperature exhibits deterministic dynamics with a low-dimensional structure (1.995383), consistent with Module 4 attractors (32-33°C). Humidity's dimension (1.866193) suggests deterministic dynamics but possible noise (close to surrogate 1.978875). Hive Power's dimension (1.384295) indicates deterministic dynamics, with a value near 1 suggesting periodicity (Limit Cycle, Module 5, P6). However, its phase space plot did not show a smooth closed trajectory, possibly due to quasi-periodicity (multiple frequencies, Module 5, P7) or mixed dynamics (periodic baseline with non-periodic bursts). Future work includes refining τ for hive power, reducing noise in humidity, and exploring multi-view embedding.

Humidity Corr. Dim. Sensitivity (Surrogate)

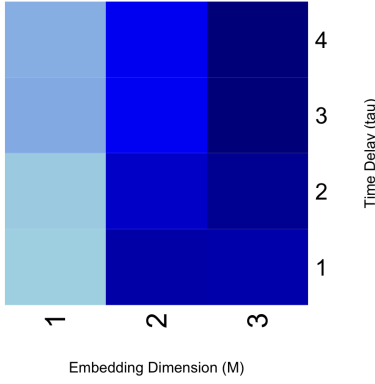


Figure 9: Sensitivity Analysis Heatmap for Humidity (Surrogate)

Temperature Phase Space

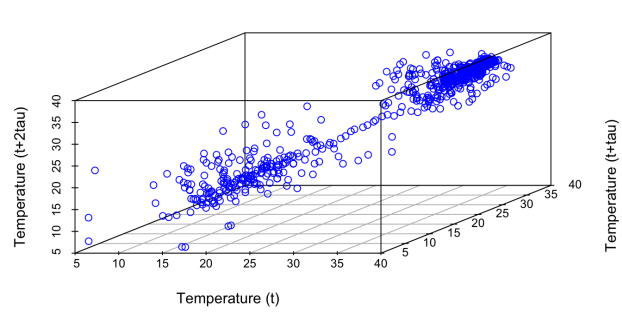


Figure 12: Temperature Phase Space Plot ($\tau = 2$, $M = 6$, 3D)

Hive Power Corr. Dim. Sensitivity (Original)

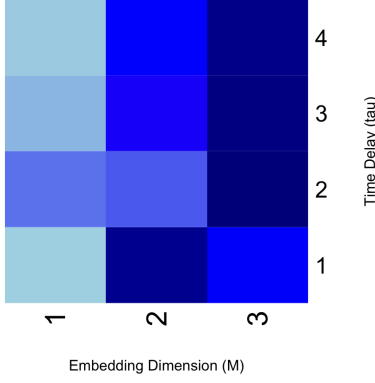


Figure 10: Sensitivity Analysis Heatmap for Hive Power (Original)

Humidity Phase Space (2D)

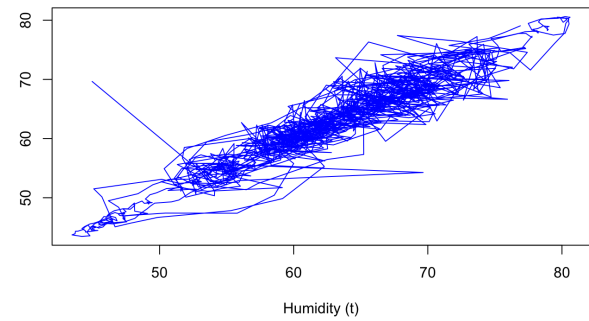


Figure 13: Humidity Phase Space Plot ($\tau = 2$, $M = 2$, 2D)

Hive Power Corr. Dim. Sensitivity (Surrogate)

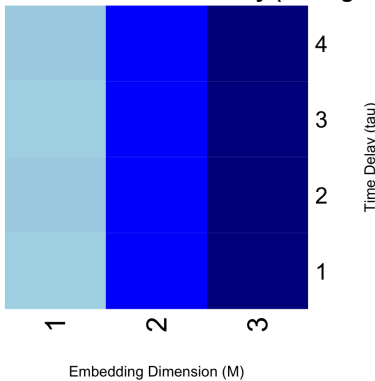


Figure 11: Sensitivity Analysis Heatmap for Hive Power (Surrogate)

Hive Power Phase Space (2D)

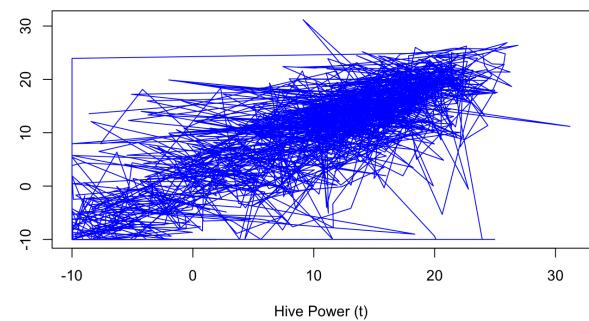


Figure 14: Hive Power Phase Space Plot ($\tau = 2$, $M = 2$, 2D)

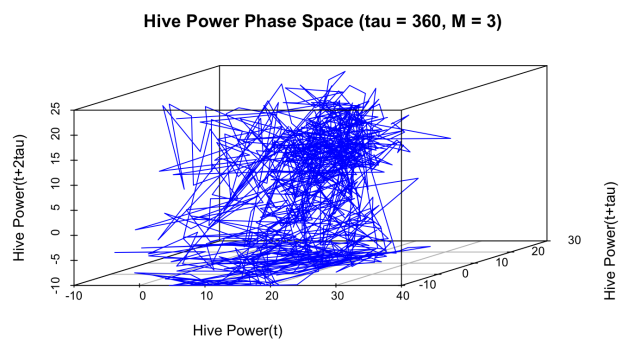


Figure 15: Hive Power Phase Space Plot ($\tau = 360$, $M = 3$,
3D, First 200 Points)

Multivariate Recurrence Analysis

ePortfolio Entry 4 - Module 6

Group 6: Djourdan Johnson, Jacuqot Qiu, Lotte Michels, Nawat Nawati Azhati, Nuo Xu, Xuelin Wei

1 Introduction

In this project, we conducted a detailed recurrence-based time series analysis of Hive 202204, focusing on the summer segment of the dataset collected from the MSPB database (Zhu et al., 2023). Our objective was to investigate the temporal dynamics between acoustic and thermal environmental data recorded inside the hive.

We primarily employed Recurrence Quantification Analysis (RQA) and Classical Cross Recurrence Quantification Analysis (CRQA) to explore the behavioral dynamics of the hive during the summer (Wallot & Leonardi, 2018; Wallot, 2019), and we compared the differences in RQA results before and after detrending. Principal Component Analysis (PCA) and K-means clustering were also used as complementary methods to classify temporal dynamic patterns.

We focused on three key signals—temperature, hive power, and humidity—all of which are indicative of colony activity levels and stress conditions.

The code used for the computations and visualizations in this entry can be found [here](#).

2 Data Preprocessing

Given that the RQA method does not require assumptions of distributional form or stationarity and is robust to outliers, we first removed duplicate timestamps, eliminated missing values, and standardized all three variables (Wallot & Leonardi, 2018). We also verified that the three variables shared a consistent sampling frequency, aligned the time series accordingly, and excluded extreme outliers. Due to irregular sampling and a high proportion of missing values at the beginning and end of the recordings (Zhu et al., 2023), we removed these time segments to ensure data quality.

Short gaps within the selected time window were handled automatically using `.dropna()`, and since all variables were uniformly resampled at 15-minute intervals, these gaps were smoothed without disrupting temporal continuity or synchrony.

As a result, the cleaned dataset retained sufficient temporal integrity to support valid CRQA analysis.

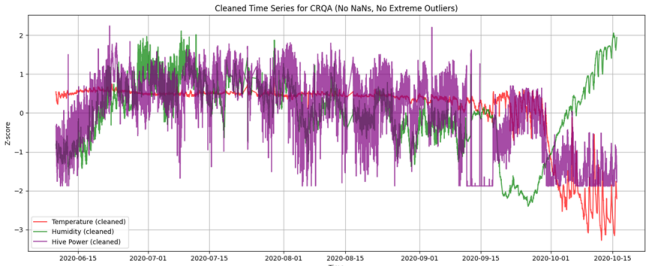


Figure 1: Cleaned Time Series for CRQA

3 Univariate RQA

To characterize the internal dynamics of Hive, we conducted univariate RQA analyses on each of the individual signal variables. We employed embedding parameters recommended by the Delayed Mutual Information (DMI) and False Nearest Neighbors (FNN) methods (Wallot & Mønster, 2018). We obtained the following RQA measures:

Signal	m	r
temperature_z	47	6
humidity_z	42	6
hive_power_z	20	7

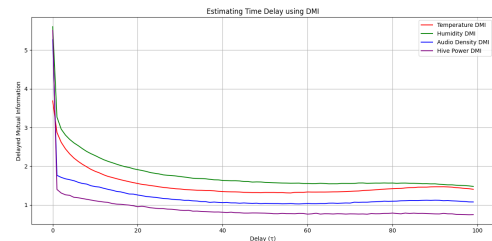


Figure 2: Estimating Time Delay using DMI

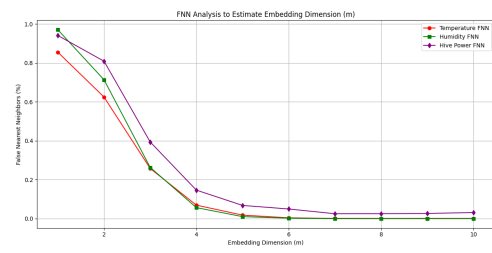


Figure 3: FNN Analysis to Estimate Embedding Dimension

	temperature_z	humidity_z	hive_power_z
RR	0.179877	0.098953	0.108894
DET	0.981573	0.925347	0.717501
L	17.33446	8.568472	3.889255
L_max	2500	2822	526
DIV	0.0004	0.000354	0.001901
L_entr	3.48672	2.613604	1.741879
LAM	0.987129	0.955045	0.809494
TT	26.17579	13.08573	5.335198
V_max	1101	783	553
V_entr	3.737406	2.950859	2.103107
W	126.9318	117.0331	38.05462
W_max	11104	10583	11057
W_div	9.00E-05	9.40E-05	9.00E-05
W_entr	3.714394	3.715002	3.074755
DET/RR	5.456905	9.351356	6.588961
LAM/DET	1.00566	1.032094	1.128214

Table: RQA Summary (Variables as Rows)

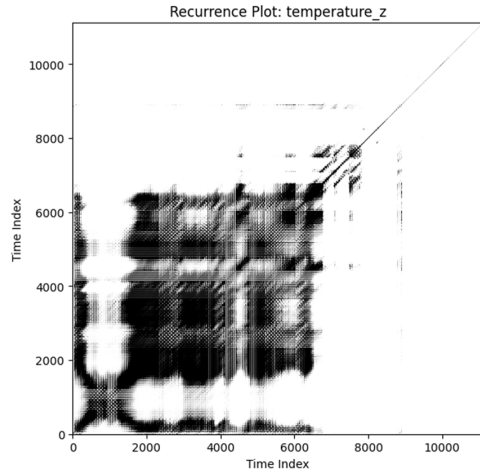


Figure 4: Recurrence Plot: Temp_z

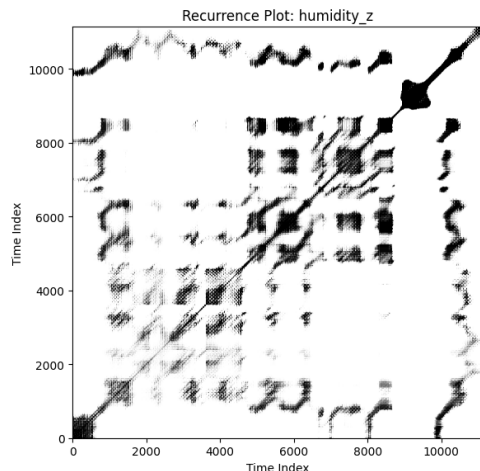


Figure 5: Recurrence Plot: humidity_z

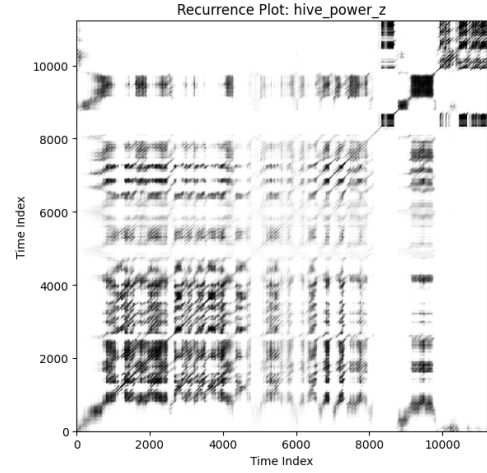


Figure 6: Recurrence Plot: hive_power_z

The recurrence plot of temperature is densely populated and well-structured, with repeated motifs and clear diagonals, indicating strong self-similarity and stable cyclicity. This is supported by its RQA metrics: RR = 17.99%, DET = 98.16%, LAM = 98.71%. This suggests temperature is a highly regulated and stable variable in the hive.

In contrast, the recurrence plot of humidity is sparser, with irregular bands and fewer diagonals. Although DET is relatively high (92.53%), the lower RR (9.90%) indicates fewer recurring states. A dense region in the latter part suggests external influences or regime shifts. Humidity shows some temporal coherence but is more susceptible to environmental fluctuations. The recurrence plot of hive_power is most fragmented, lacking clear patterns, with high variability. This is reflected in its metrics: DET = 71.75%, RR = 10.89%. This aligns with its role as a proxy for behavioral fluctuations in hive activity. Overall, the variables show a stability hierarchy: temperature, humidity, hive power. This reflects differing levels of regulation and sensitivity to external factors.

To avoid long-term trends obscuring dynamic structure, we detrended all signals. As shown in rolling means, temperature declines sharply after mid-September, while humidity and hive_power fluctuate throughout. If unremoved, these trends could distort recurrence metrics or inflate determinism. Detrending improves the accuracy of recurrence analysis by focusing on short-term structure.

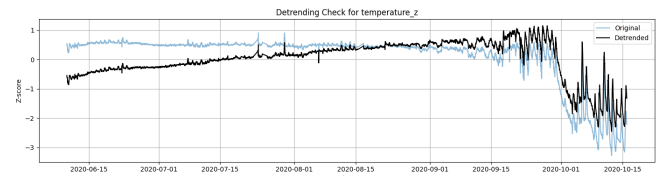


Figure 7: Detrending Check for temperature_z

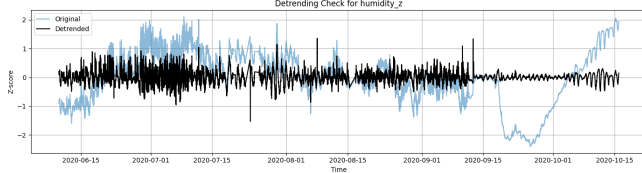


Figure 8: Detrending Check for humidity_z

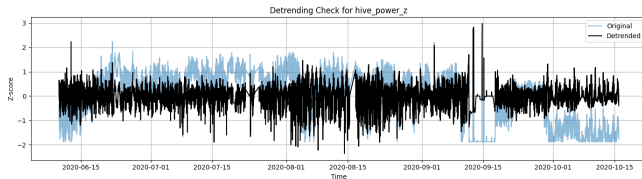


Figure 9: Detrending Check for hive_{power}_z

	[H]		
RR	0.034926	0.819903	0.488145
DET	0.980671	0.981251	0.862554
L	17.68371	17.6754	5.224522
L_max	2500	2822	526
DIV	0.0004	0.000354	0.001901
L_entr	3.351397	3.14273	2.157038
LAM	0.986793	0.988008	0.90282
TT	26.01152	28.42331	7.449154
V_max	1011	2822	680
V_entr	3.672196	3.415477	2.490389
W	694.8218	7.853371	8.309424
W_max	11104	7373	8503
W_div	9.00E-05	0.000136	0.000118
W_entr	4.412869	2.447347	2.433745
DET/RR	28.07891	1.196789	1.767003
LAM/DET	1.006242	1.006886	1.046682

Table: Detrended RQA Summary

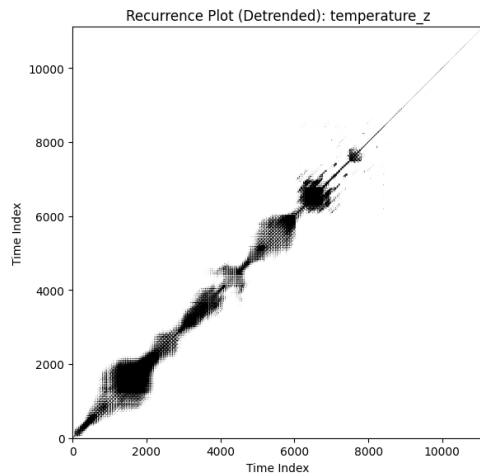


Figure 10: Recurrence Plot (Detrended): temperature_z

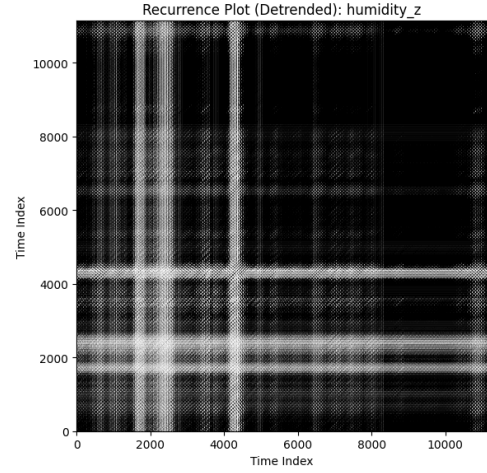


Figure 11: Recurrence Plot (Detrended): humidity_z

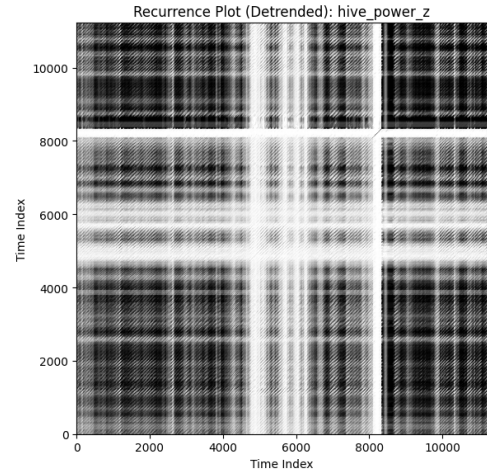


Figure 12: Recurrence Plot (Detrended): hive_{power}_z

To extract genuine dynamical patterns, we repeated the RQA after removing low-frequency trends. The results show that detrending removed nonstationary components while preserving or enhancing meaningful recurrence features. For temperature, RR dropped (17.99 to 3.49%) while DET and LAM remained high (98.07%, 98.68%), indicating genuine cyclic structure. For humidity, the recurrence became highly repetitive (RR: 81.99%), with DET and LAM staying high, suggesting enhanced regularity and periodicity. For hive power, RR rose to 48.81% and DET increased from 71.75% to 86.26%, revealing latent behavioral structures. Notably, even with a fixed radius of 0.7, the high RR values for humidity and hive power indicate pronounced short-term recurrence after detrending, potentially reflecting cyclic regulation or collective behavioral rhythms.

Overall, detrending improved the interpretability of recurrence plots by emphasizing short-term structural dynamics.

4 CRQA Results

For CRQA analysis we selected the parameters $m = 7$ and $\tau = 33$. To ensure that the recurrence matrix captured sufficient

recurrence without becoming overly saturated, we conducted a sweep analysis of RR across different radius values. The optimal radius was found to be 0.6, where the RR fell within the interpretable range of 2–10

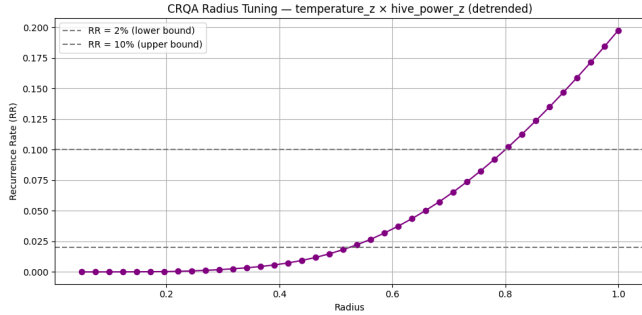


Figure 13: CRQA Radius Tuning

We obtained the following key metrics:

CRQA Metrics	Value
Recurrence rate (RR)	0.099899
Determinism (DET)	0.700436
Average diagonal line length (L)	3.905308
Longest diagonal line length (L_max)	50
Divergence (DIV)	0.02
Entropy diagonal lines (L_entr)	1.768985
Laminarity (LAM)	0.700744
Trapping time (TT)	3.916318

CRQA Metrics

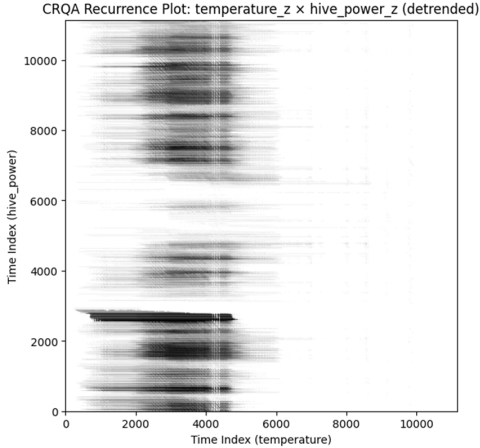


Figure 14: CRQA Recurrence Plot: temperature_z × hive_power_z (detrended)

To assess the dynamic relationship between hive temperature and acoustic activity, we performed CRQA on the detrended temperature and hive_power signals. The cross-recurrence plot shows horizontal banding in the lower and middle regions, indicating that hive power recurs in alignment with temperature at specific time lags. The recurrence rate (RR = 9.99%) suggests moderate shared state space, while determinism (DET = 70.04%) indicates short-lived coordination patterns. Low diagonal length ($L = 3.91$) and entropy, along

with LAM = 70.07% and TT = 3.92, suggest that alignment is local and episodic.

In sum, CRQA reveals structured but non-persistent coupling between temperature and hive acoustic signals.

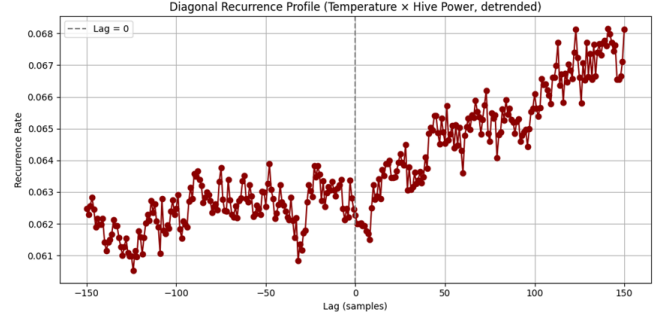


Figure 15: Diagonal Recurrence Profile

To further examine the temporal relationship between hive temperature and acoustic activity, we computed a Diagonal Recurrence Profile (DRP) based on the cross-recurrence matrix of the detrended temperature and hive_power signals.

The DRP quantifies the recurrence rate (RR) along diagonals offset by varying time lags, thereby revealing whether one signal systematically precedes or follows the other in terms of shared dynamic states.

The DRP curve, constructed with a maximum lag of 150 samples, exhibits a clear upward trend toward positive lags, indicating that hive power aligns more frequently with earlier states in temperature. In other words, temperature changes tend to precede shifts in hive acoustic energy. This asymmetric profile implies that temperature may be a leading indicator of behavioral changes rather than occurring concurrently.

5 Windowed CRQA and Local DRP

To assess how the dynamic coupling between hive temperature and acoustic activity evolves over time, a windowed CRQA was performed on the detrended temperature and hive_power signals.

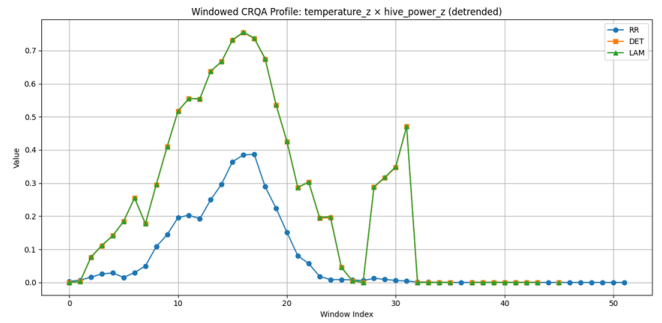


Figure 16: Windowed CRQA Profile: temperature_z × hive_power_z (detrended)

The signals were segmented into overlapping windows, and CRQA metrics—including recurrence rate (RR), determinism (DET), and laminarity (LAM)—were computed within each window to capture temporal variations in coordination.

The resulting profile reveals a clear phase of elevated interaction between window indices 10 and 20. RR peaks near window 17 (0.39), and both DET and LAM exceed 0.75, indicating strongly structured joint dynamics.

In contrast, beyond this phase—especially after window index 30—all three metrics decline sharply, suggesting a breakdown in coordination between the signals. A secondary peak appears near window 31, but it is brief and less coherent.

These results indicate that the coupling between temperature and hive acoustic energy is not constant, but fluctuates, with a distinct phase of strong synchronization likely reflecting coordinated behavioral or regulatory activity within the hive.

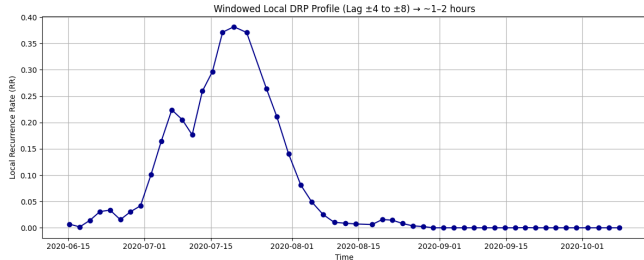


Figure 17: Windowed Local DRP Profile (Lag ± 4 to ± 8) \rightarrow 1–2 hours

To examine the temporal evolution of short-lag coupling between hive temperature and acoustic activity, a windowed local diagonal recurrence profile (local DRP) was computed using a lag range of ± 4 to ± 8 samples (1–2 hours). This profile captures localized recurrence rates (RR) across successive time windows, identifying when short-lag alignment is strong or weak.

The resulting profile reveals a distinct peak in recurrence around mid-July 2020, with RR peaking at 0.38, indicating strong short-lag temporal alignment. This peak is preceded by a gradual increase from late June and followed by a steady decline through August. After early August, the RR drops to near zero and remains flat through September and October, suggesting the short-term relationship faded. This analysis shows that short-lag coordination between temperature and hive power is temporally localized, occurring mainly in early to mid-summer. The strong recurrence likely reflects coordinated thermoregulation or collective behaviors that dissipate with seasonal changes or hive condition shifts.

6 PCA and KMeans Clustering

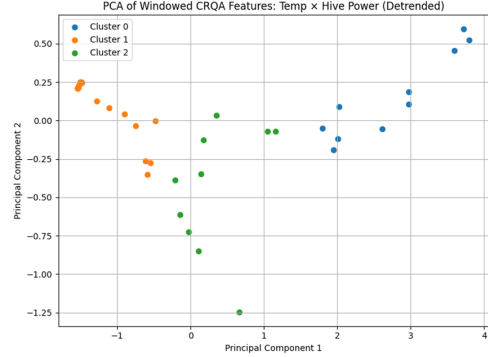


Figure 18: PCA of Windowed CRQA Features

To identify distinct temporal regimes in the interaction dynamics between hive temperature and hive acoustic energy, we performed k-means clustering on windowed CRQA features (RR, DET, LAM) extracted from detrended signals.

The resulting clusters were visualized using Principal Component Analysis (PCA), and their feature-wise means are summarized in the accompanying table.

Three distinct clusters emerged: Cluster 0 (blue, 10 windows): High recurrence (RR = 0.2786), moderate DET and LAM (0.636), indicating strong and structured coordination.

Cluster 1 (orange, 24 windows): Minimal RR (0.0081), nearly zero DET and LAM (0.047), corresponding to uncoordinated or decoupled dynamics.

Cluster 2 (green, 10 windows): Moderate RR (0.0602), intermediate DET and LAM (0.34), possibly reflecting transitional behavior between states.

These findings confirm that the temperature–hive power relationship is temporally structured, fluctuating between phases of strong synchrony, weak coupling, and transitions.

The clustering highlights discrete dynamical states in the hive system and their temporal evolution.

Cluster	RR	DET	LAM	PC1	PC2
0	0.2786	0.636	0.637	2.7414	0.1547
1	0.0081	0.0471	0.0475	-1.2775	0.1188
2	0.0602	0.3396	0.3403	0.3246	-0.4399

Table: Cluster Summary of Windowed CRQA Features

7 Conclusion

This study applied Recurrence Quantification Analysis (RQA), Cross-Recurrence Quantification Analysis (CRQA), Diagonal Recurrence Profile (DRP), and their multivariate extensions to systematically investigate the dynamic coupling between hive temperature and acoustic energy.

We found that determinism (DET) and recurrence rate (RR) were the most informative indicators, effectively differentiating between periodic regulation, decoupled states, and transitional dynamics.

Windowed analysis and clustering revealed three discrete dynamical phases—synchronization, decoupling, and transition—showing that coupling is temporally localized rather than persistent.

DRP results indicated that temperature changes tend to precede acoustic activity, suggesting temperature as a potential leading indicator of behavioral coordination.

In conclusion, recurrence-based methods not only revealed the complex nonlinear coupling between hive temperature and acoustic energy, but also provided an effective framework for detecting dynamic state transitions in ecological behavioral systems.

References

1. Analyzing multivariate dynamics using cross-recurrence quantification analysis (CRQA), diagonal-cross-recurrence profiles (DCRP), and multidimensional recurrence quantification analysis (MdRQA): A tutorial in R. *Frontiers in Psychology*, 9, 2232.
2. Calculation of average mutual information (AMI) and false-nearest neighbors (FNN) for the estimation of embedding parameters of multidimensional time series in Matlab. *Frontiers in Psychology*, 9, 1679.
3. Multimodal sensor data of honey bee colonies: From univariate statistics to complex systems analysis. *Patterns*, 4(6), 100779.

Surrogate Testing

ePortfolio Entry 5 - Module 7

Group 6: Djourdan Johnson, Jacuqot Qiu, Lotte Michels, Nawat Nawati Azhati, Nuo Xu, Xuelin Wei

1 Checking for Result Significance

Throughout this project, we apply a variety of methods to characterize the dynamics of a honeybee colony as a complex system. In general, complex systems often produce data that look complicated, but sometimes simple stochastic processes or linear correlations can mimic complexity measures. Surrogate testing guards against mistaking such processes for complexity.

Specifically, surrogate testing shows whether that metric is statistically significant against a well-defined null model. The core idea is to generate proxy data and calculate a metric of interest on this data. These steps are typically repeated 20 times to generate a distribution of surrogate metric scores (Kantz and Schreiber, 2004). The true metric is then compared against this distribution using inferential statistics to assess its significance. This is fundamental in complexity science because it helps distinguish genuine complex dynamics from simpler or random processes.

Moulder et al. (2018) propose various ways to generate surrogate time-series, each depending on its own null hypothesis (H_0):

1. **Data Shuffling:** randomizing the order of values in a signal (without replacement). H_0 = there is no temporal structure within a time-series/there is no time dependency between two or more time-series.
2. **Amplitude Adjusted Fourier Transform (AAFT):** randomizing time-series while preserving the original amplitude distribution and linear autocorrelation. This method was originally proposed by Theiler et al. (1992). It tests the same null hypothesis as data shuffling.
3. **Segment Shuffling:** cutting the data into a number of segments and randomizing the order of these segments. H_0 = there is no time dependency between randomly paired segments (of a certain size) for two or more time series.
4. **Data Sliding:** splitting the data in two and appending the latter part to the beginning of the time-series.

H_0 = Long lags between two time series do not influence their time dependency.

5. **Participant Shuffling:** interchanging time-series between interactive and non-interactive signal pairs, for instance over different subjects in the data. H_0 = the observed measure between series is no different between interactive and non-interactive pairs.

For the beehive within the MSPB data (Zhu et al., 2024), the first four surrogate analysis methods are applicable. Figure 1 roughly visualizes how these methods create surrogate signals, applied to the raw humidity signal. The methods will be further explained and demonstrated by assessing the significance of the recurrence metrics found in the previous ePortfolio entry (entry 4/module 6). The exact pre-processing steps and parameter settings from this module will be re-used to ensure fair surrogate tests. The code used for these analyses can be found [here](#). To keep this module concise, we will restrict ourselves to three metrics of interest: the recurrence rate (RR), determinism (DET) and laminarity (LAM).

2 Univariate Surrogate Testing for RQA

In module 6, the univariate recurrence within the hive power, humidity and temperature signals were examined using recurrence quantification analysis (RQA). A summary of the original results is provided in Table 1. The robustness of these results was assessed using data shuffling and AAFT. These approaches were implemented as Python functions and applied to all three signals.

Signal	Original RQA Metrics		
	RR	DET	LAM
Temperature	0.180	0.982	0.990
Humidity	0.099	0.925	0.955
Hive Power	0.109	0.718	0.809

Table 1: Original Recurrence Quantification Analysis (RQA) results per signal, computed in Entry 4/Module6. RR = Recurrence Rate, DET = Determinism, LAM = Laminarity.

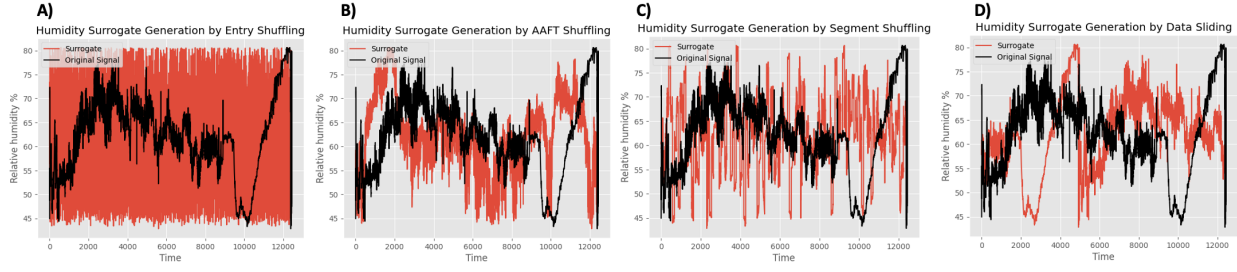


Figure 1: Example surrogate signals for the raw humidity time-series. Different methods are displayed. A: Data shuffling B: AAFT shuffling. C: Segment shuffling, with a segment size of 96 timepoints. D: Data sliding, with a cut-off at 60% of the data.

2.1 Data Shuffling

Surrogate time-series were created for all three signals by randomizing the order of the constituent values (Moulder et al., 2018). As such, temporal properties within the sequences are destroyed. Next, RQA was performed on the surrogate signals, using the same parameters as for the original signals (see previous ePortfolio entry). This process was repeated 20 times, as recommended by Kantz and Schreiber (2004), to create a distribution of surrogate RQA results.

Based on these acquired distributions, a mean and 95% confidence interval (CI) for the recurrence metrics of interest were computed. The results are displayed in Table 2. Data shuffling, in this case, is conducted to test the null hypothesis that *there is no temporally recurrent structure within the time-series of interest*. If the original metric falls outside of the surrogate CI, that null hypothesis can be rejected. Alternatively, if the original metric falls within the surrogate CI, the null hypothesis cannot be rejected and the recurrence metric may not be significant.

Combined, tables 1 and 2 show that the true RQA metrics fall outside of the surrogate confidence intervals. Data shuffling surrogates thus reject the null hypotheses for all variables and conclude that the RQA metrics in Table 1 are significant.

2.2 Amplitude Adjusted Fourier Transform

Data shuffling suggest the original metrics to be significant. However, to make our findings even more robust, we can apply multiple surrogate generation techniques and compare their outcomes. In contrast to the data shuffling technique, Amplitude Adjusted Fourier Transform (AAFT) is designed to generate surrogate sequences that ensure a Gaussian distribution and maintain some original signal features like the mean and autocorrelation (Moulder et al., 2018; Theiler et al., 1992). As such, AAFT generated sequences may be more plausible surrogates for a signal. This can also be viewed in Figure 1 when comparing plots A and B.

To implement AAFT, functionalities were used from the pyunicorn package (Donges et al., 2016). Like before, 20 surrogates were created and submitted to RQA, using the original parameters. Again, metric means and 95% confidence intervals (CIs) were computed, as displayed in Table 3.

AAFT surrogates test the same null hypothesis as data shuffling. Hence, the same decision rules apply regarding the statistical significance of the original metrics. Thus, juxtaposed to Table 1, the AAFT results show that the true RQA metrics for temperature and humidity are significantly higher than expected under the null hypothesis. For temperature and humidity, AAFT surrogates thus reject the null hypothesis that these signals feature no temporally recurrent structure.

This is not the case for the power signal: for all three recurrence metrics, tables 1 and 3 indicate that the original power signal scores significantly lower than the AAFT surrogate results. The power signal may thus be less recurrent, deterministic and laminar than expected under the null hypothesis. The observed RQA metrics in the power signal are not robust.

3 Bivariate Surrogate Testing for CRQA

So far, it was demonstrated that data shuffling and AAFT can be applied to effectively assess the significance of univariate RQA. These methods can also be applied to check the robustness of bi- or multivariate findings. However, it should be noted that data shuffling and AAFT largely get rid of any temporal properties (Moulder et al., 2018). As a result, surrogate signals may not adhere to certain contextual aspects. For instance, regarding beehives, Zhu et al. (2024) describe that the dynamics in honeybees show typical daily cycles (following a 'biological clock'). Such biological constraints are lost in AAFT and data shuffling, which can cause null hypotheses to be rejected too easily in a bi- or multivariate scenario.

To avoid such spurious findings, Moulder et al. (2018) define two alternative and more plausible surrogate meth-

Metric	Temperature			Humidity			Power		
	Mean	Lower CI	Upper CI	Mean	Lower CI	Upper CI	Mean	Lower CI	Upper CI
RR	0.0043	0.0042	0.0044	0.00267	0.0026	0.0027	0.0069	0.0068	0.0070
DET	0.0080	0.0073	0.0087	0.0051	0.0049	0.00522	0.0135	0.0131	0.0139
LAM	0.0532	0.0490	0.0575	0.0119	0.0109	0.0129	0.0346	0.0332	0.0361

Table 2: **Data shuffling** surrogate RQA metrics per signal. Each metric is characterized by the mean and 95% confidence interval of its surrogate distribution. For each variable, the original metrics are significantly higher than the surrogate mean.

Metric	Temperature			Humidity			Power		
	Mean	Lower CI	Upper CI	Mean	Lower CI	Upper CI	Mean	Lower CI	Upper CI
RR	0.1159	0.1077	0.1242	0.0533	0.0504	0.0562	0.1716	0.1686	0.1746
DET	0.9555	0.9512	0.9597	0.8410	0.8322	0.8497	0.9365	0.9342	0.9387
LAM	0.9721	0.9695	0.9747	0.8961	0.8907	0.9015	0.9569	0.9553	0.9585

Table 3: **AAFT** Surrogate RQA metrics per signal. Each metric is characterized by the mean and 95% confidence interval of its surrogate distribution. For temperature and humidity, all original metrics are significantly higher than the surrogate mean. For hive power, all original metrics are significantly lower than the surrogate mean.

ods: segment shuffling and data sliding. These techniques can be employed to check the significance of the cross-RQA (CRQA) results described in the previous ePortfolio entry on module 6. For that module, the pairwise cross-recurrence between the detrended temperature and hive power signals was explored. With regards to the metrics of interest, the following results of were found: RR = 0.023, DET = 0.537, LAM = 0.537 (also reported in tables 4 and 5).

Bi-variate surrogate tests can further assess these results. For each of those tests, a surrogate signal is created for the detrended temperature, while the un-shuffled version of the detrended hive power timeseries was used.

3.1 Segment Shuffling

Segment shuffling entails that timeseries are divided into smaller, separate chunks (Moulder et al., 2018). These chunks are randomly shuffled among each other, while the temporal order within chunks is retained. For the detrended temperature signal, a segment size of 199 timepoints was selected: segments represented almost 50 hours (a bit more than two days) in the data. This segment size could evenly divide the timeseries into 57 chunks and takes the day cycles described by Zhu et al. (2024) into account. The chunks were cut, put in random order and concatenated again to create a segment shuffled surrogate signal. This process was iterated 20 times, to create 20 of such surrogates for the detrended temperature signal.

Next, the surrogate temperature signals were coupled

with the power signal and inputted to pairwise CRQA, using the same parameters as for the original computation (see previous ePortfolio entry). This resulted in a distribution of 20 CRQA measurements. Subsequently, means and 95% confidence intervals (CIs) for each surrogate recurrence metric of interest were computed. The results are displayed in Table 4. Segment shuffling, in our case, is employed to test the null hypothesis that *there is no time dependency between randomly ordered days for two time-series*. Whether the original metric falls out- or inside of the surrogate CI determines whether, respectively, this null hypothesis is rejected or not.

The segment surrogate results indicate that all the original recurrence metrics are significant. That is, the coupling of temperature and hive power shows higher recurrence, determinism and laminarity than expected under the null hypothesis. Segment surrogates thus reject this null hypothesis.

Metric	Original	Surrogate Results		
		Lower CI	Upper CI	Mean
RR	0.09989	0.057	0.055	0.059
DET	0.700	0.590	0.576	0.602
LAM	0.701	0.599	0.586	0.611

Table 4: **Segment shuffling** surrogate results for the CRQA between the (detrended) temperature and hive power signals.

3.2 Data Sliding

Instead of dividing signals into multiple chunks, data sliding entails that a time-series is split in two and that the order of the two parts is switched (Moulder et al., 2018). Whereas segment shuffling thus maintains small and local temporal trends, data sliding can be applied to take larger and more global temporal lags into account.

Moulder et al. (2018) suggest that signals are split around 60%. In addition, Kantz and Schreiber (2004) propose that surrogate testing is repeated 20 times to create a surrogate distribution of outcomes as a statistical benchmarking baseline. We combined both recommendations. First, 20 cut-off points were randomly sampled between 50% and 70%. The signal parts created by these cut-offs were then swapped, creating 20 data sliding surrogate timeseries. This process was conducted for the detrended temperature signal, while again keeping the hive power time-series fixed.

The resulting sequences were submitted to the pairwise CRQA computation from module 6, again using the same parameters as for the original analysis (see previous ePortfolio entry). Once more, means and 95% CIs were computed for each surrogate recurrence metric. The results are displayed in Table 5. Data sliding tests the null hypothesis that *long lags between two time series do not influence their time dependency*. Whether the original metric falls out- or inside of the surrogate CI statistically determines whether, respectively, this null hypothesis is rejected or not.

Contrasted to the original results, Table 5 indicates that the original recurrence rate and determinism results for CRQA are significantly higher than expected under the null hypothesis. This suggests that the recurrence and determinism between the (detrended) temperature and power signals is not influenced by long lags. Moreover, laminarity was not found to be as robust as the other two metrics. Table 5 indicates that the original LAM result is significantly lower than the surrogate outcomes. The coupling between temperature and hive power may thus be less laminar than expected under the null hypothesis.

To slightly nuance these findings, it should be noted that the original and surrogate results for data sliding (Table 5) are very close to each other, especially compared to the segment surrogate tests (Table 4).

4 Surrogate Testing for Windowed CRQA

The previous ePortfolio entry further explored the cross-recurrence between the detrended temperature and power signals by applying windowed CRQA. Specifically, a 1000 timepoint window size and 200 timepoint step size were used to obtain CRQA results for smaller, local patches in the signals. The windowed results were visualized to show the changes in cross-recurrence over

Metric	Original	Surrogate Results		
		Lower CI	Upper CI	Mean
RR	0.09989	0.09977	0.09968	0.09986
DET	0.700	0.693	0.687	0.699
LAM	0.7007	0.701	0.7009	0.7019

Table 5: **Data sliding** surrogate results for the CRQA between the (detrended) temperature and hive power signals.

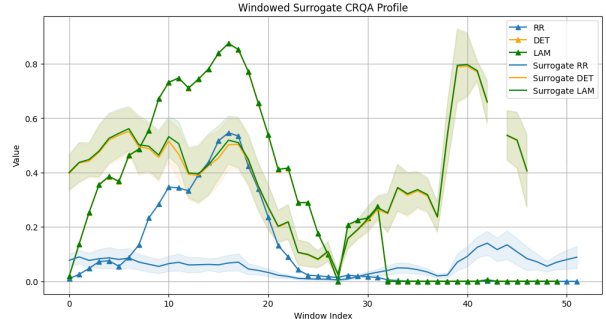


Figure 2: Windowed surrogate CRQA results against the original CRQA results (dotted). Surrogate sequences are wrapped by 95% CI areas.

time. This plot revealed several peaks in cross-recurrence between detrended temperature and power around.

To assess the robustness of these findings, windowed surrogate testing was applied. The segment shuffled surrogate signals generated in the previous section were used were for this task. For each surrogate, the original sliding window (described before) was applied to compute the surrogate CRQA over time. Thus, 20 sequences of windowed surrogate CRQA results were obtained. The mean and 95% CI of these sequences are displayed in Figure 2, plotted against the original windowed CRQA profile.

This figure shows that small recurrence peaks in the original profile may not be robust. They either fall within the surrogate CI or are surpassed by the surrogate outcomes. The large peak on the left of the plot, however, shows significantly higher values for the original recurrence metrics compared to the surrogate signals. The underlying windows correspond to the time period ranging from around the end of June to the beginning of August. This peak in temperature-power cross-recurrence may thus forebode thermoregulatory behavior shown by beehives as they transition from colder to warmer weather (Research and Consortium, 2010). Additional analyses in our ePortfolio, such as the Dynamic Time Warping approach in Entry 6/Module 8, will further delineate this phenomenon.

5 Conclusion

Surrogate testing is important in complexity science to avoid false positive findings by creating a null model that complex measures can be benchmarked against. Various surrogate testing approaches were applied and compared to check the robustness of RQA findings from Entry 4/Module 6 of our ePortfolio. Data shuffling and AAFT surrogates suggested that temperature and humidity exhibit significant recurrence. In contrast, AAFT indicated that recurrence in beehive power was not as robust.

Additionally, segment shuffling and data sliding surrogates demonstrated the robustness of the cross-recurrence between the temperature and hive power. Solely the laminarity metric was found not to be resistant to long time lags in the time-series. Lastly, the CRQA was further validated with a windowed surrogate approach. The results highlighted a cross-recurrence peak between temperature and hive power around ...

References

- [Donges et al.2016] Jonathan Donges, Jobst Heitzig, Boyan Beronov, Marc Wiedermann, Jakob Runge, Qing Yi Feng, Liubov Tupikina, Veronika Stolbova, Reik Donner, Norbert Marwan, Henk Dijkstra, and Jürgen Kurths. 2016. Unified functional network and nonlinear time series analysis for complex systems science: The pyunicorn package. *EGU General Assembly Conference Abstracts*, 4.
- [Kantz and Schreiber2004] Holger Kantz and Thomas Schreiber. 2004. *Nonlinear time series analysis*. Cambridge University Press, 1.
- [Moulder et al.2018] Robert G Moulder, Steven M Boker, Fabian Ramseyer, and Wolfgang Tschacher. 2018. Determining synchrony between behavioral time series: An application of surrogate data generation for establishing falsifiable null-hypotheses. *Psychological Methods*, 23(4):757–773, 3.
- [Research and Consortium2010] Mid-Atlantic Apiculture Research and Extension Consortium. 2010. Seasonal Cycles of Activities in Colonies, 6.
- [Theiler et al.1992] James Theiler, Stephen Eubank, André Longtin, Bryan Galdrikian, and J. Doyne Farmer. 1992. Testing for nonlinearity in time series: the method of surrogate data. *Physica D Nonlinear Phenomena*, 58(1-4):77–94, 9.
- [Zhu et al.2024] Yi Zhu, Mahsa Abdollahi, Ségolène Maucourt, Nico Coallier, Heitor R. Guimarães, Pierre Giovenazzo, and Tiago H. Falk. 2024. MSPB: a longitudinal multi-sensor dataset with phenotypic trait measurements from honey bees. *Scientific Data*, 11(1), 8.

Pairwise Coordination: Rhythmic Phase Coupling and Dynamic Attractors

Entry 6 - Module 8

Group 6: Djourdan Johnson, Jacuqot Qiu, Lotte Michels,
Nawat Nawati Azhati, Nuo Xu, Xuelin Wei

Abstract

This paper describes a method for analyzing the processing of environmental sensor data, with a focus on temperature and power signals. The dynamic nature of the data is explored by constructing phase diagrams, signal localization, Hilbert transform and CPR-based analysis. This study reflects fundamental concepts from complex systems science, in particular coordination, attractor dynamics, and phase synchronization. This paper provides a foundation for further studies of system coordination.

1. Introduction

Understanding how the parts of a system coordinate over time is essential to studying complex systems [1]. We used temperature and power time series data from a single beehive, cleaned, resampled, and normalized, to extract phase features using tools such as Hilbert transforms and CRP (Continuous Relative Phase) analysis to study this synergy. These tools were first applied to fields such as sports science and psychology to study how people move or interact [3], but are now also used by scientists to analyze patterns in environmental data. We can perform the following analyses in this complex systems project: Do temperature changes and power have predictable daily cycles? Are they temporally correlated? Is this temporal relationship stable or does it change over time? Do they gradually "sync up"?

We focus on temperature and power data because they are key to understanding how the system balances energy use and environmental needs. CRP analysis allows us to plot whether these signals are always in sync or whether there is no clear pattern. These answers may help design smarter energy systems that work with natural rhythms rather than against them. The code used for the computations and visualizations in this entry can be found [here](#).

2. Data and Methods

2.1. Dataset Description

The dataset contains time series measurements of temperature and cellular power. To ensure data consistency, we selected a subset corresponding to tag number 202204 for focused analysis. The dataset was preprocessed to prepare for subsequent resampling and difference operations, select variables and clean to ensure that the analysis is consistent with the sensing object and ensure data integrity, resampling plus interpolation to facilitate subsequent spectrum and phase analysis, and use z-scores to normalize both variables, which is suitable for subsequent frequency domain analysis or comparison of relative intensities.

We analyzed the original data, analyzed the temperature and power variables, and confirmed whether there was a long-term trend of slowly rising or falling, which laid the foundation for selecting which period of time could be used as the main analysis window, and then analyzed the autocorrelation of the variables themselves. As shown in the figure, both temperature and power variables have strong autocorrelation, and we need to detrend the data for the subsequent Hilbert phase analysis or CRP analysis. The detrended ACF values are 0.849 for temperature and 0.626 for power, which are in a very suitable range and sufficient to support the use of Hilbert Transform and Continuous Relative Phase (CRP) to analyze the relationship between the two variables.

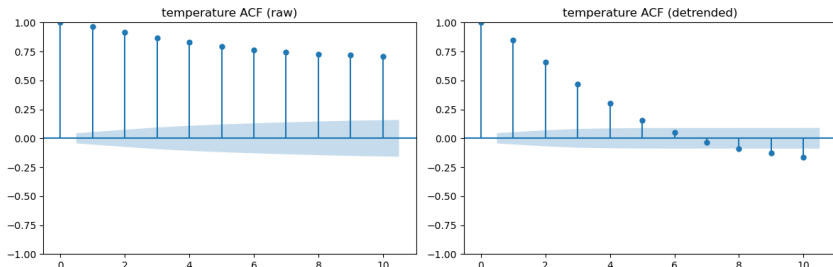


Figure 1: Centered temperature signal

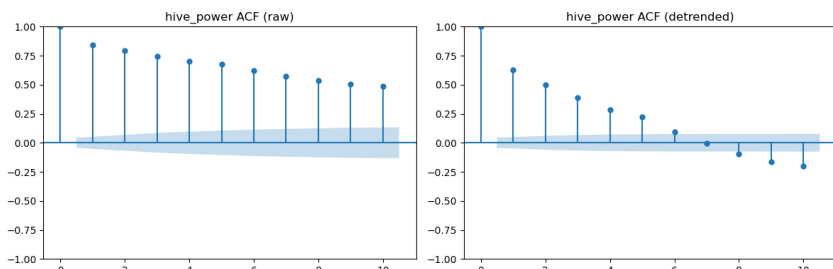


Figure 2: Centered power signal

2.2. Analytical Methods

Signal Centering: To ensure the effectiveness of the transformation and the interpretability of the synchronization indicator, we need careful signal preprocessing. Both signals are centered around zero to ensure the symmetry of the amplitude oscillation. These necessary centering processes are very important for the subsequent Hilbert analysis. A key step is signal centering. We need to subtract the mean from each time series to make it oscillate around zero.

Phase Plot: For phase map-based analysis, signals were biased to zero. This normalization is necessary to make symmetric distribution of amplitude oscillations such that a Hilbert Transform can be applied.

Hilbert Transform: To analyze the temperature and power signals, we use an analytical signal representation. (Rosenblum et al., 1996) This method allows us to compute two important values: continuous relative phase (CRP) and instantaneous phase. This allows us to study two things: (1) how the frequency and phase of the signals change over time; and (2) how the two signals interact. We assume that the result is that one signal is constantly "leading" or "lagging" the other, indicating a dynamic relationship between temperature and humidity. We then use a phase plot to visualize the phase difference and show how the signal behavior changes over time.

CRP: We will use this method to focus on the temporal relationship between temperature and power and use a tool to compute the difference between the instantaneous phase of temperature and power. We scale the data to the range $[-180^\circ, +180^\circ]$, which tells us whether the two signals are in sync or out of sync, and whether they are leading or lagging each other. If the CRP stays close to 0° , the signals are highly in sync. If the CRP fluctuates between -180° and $+180^\circ$, the signals are out of sync. This analysis clearly reveals how temperature and humidity interact in real-world environments.

Visualization: CRP curves, histograms, and phase portraits were used to explore synchronization and attractor-like dynamics.

3. Results and Analysis

3.1. Signal Centering

Centralization principle: Signal centralization is a key step in phase analysis. Its core principle is to meet the basic assumptions of the Hilbert transform: the input signal should be narrow-band and symmetrically oscillate around the zero point. Raw sensor data often has DC offsets, such as long-term high temperatures, which will destroy the symmetry of the signal and cause discontinuities or systematic deviations in phase estimation [4]. The essence of centralization processing is "data zeroing" - by subtracting the overall mean, eliminating sensor calibration errors and environmental baseline drift,

so that the signal only retains the real dynamic fluctuations. Just like shielding the background noise to hear the content of the conversation, the centralized signal can reveal the synchronization relationship between temperature and power, making the subsequent phase calculation and CRP analysis more accurate and reliable. For example, a signal with a temperature fluctuation between -3°C and $+3^{\circ}\text{C}$ and a mean of 28°C will become a symmetrical signal fluctuating between -3°C and $+3^{\circ}\text{C}$. This transformation emphasizes the relative dynamic characteristics, which is crucial for detecting synchronization patterns. Without proper centering, continuous relative phase (CRP) analysis can be confounded by inconsistent signal baselines, creating spurious phase shifts that make it look like the two signals are out of sync when they are just starting from different points. The purpose of centering is to pull the two signals back to the same starting line, ensuring that their comparison in phase space is fair.

Normalization involves centering, but also scaling by the standard deviation. For Hilbert analysis, centering is required, but normalization is optional. If the noise is dominant in the high-frequency range, filtering should be performed first to avoid biasing the mean estimate due to transients or outliers. To illustrate the effect of centering, Figure 3 shows the removal of baseline shifts by comparing the original temperature signal and the centered temperature signal with a horizontal zero line. Figure 4 shows the complex plane representation of the Hilbert transformed signal, where the real axis reflects the centered signal and the imaginary axis reflects the orthogonal components, showing the circular or elliptical shapes required for phase continuity.

In the analysis, centering improves CRP estimates by accurately extracting the instantaneous phase in the temperature and power signals. This preprocessing step makes the synchronization patterns we observe clearer and thus less likely to be misleading.

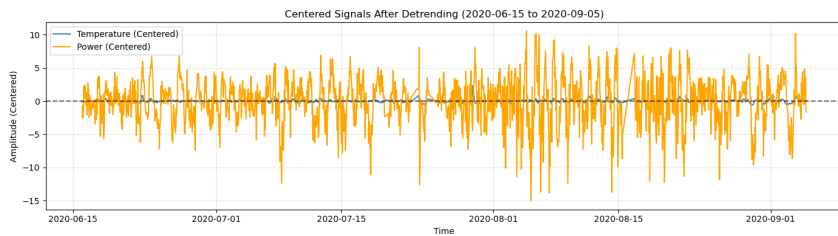


Figure 3: Centered Signals After Detrending

3.2. Phase Portraits

phase plot of the temperature signal reveals a clear attractor-centered dynamical structure. The phase plot of the detrended temperature signal reveals a stable, center-centered dynamical structure. Most of the data points are concentrated near the origin $(0, 0)$, where the detrended temperature is close to zero and the rate of change is minimal. Occasional deviations from this center, reflected in scattered points far from the origin,

Figure 2: Complex Plane of Hilbert Transform (Temperature)

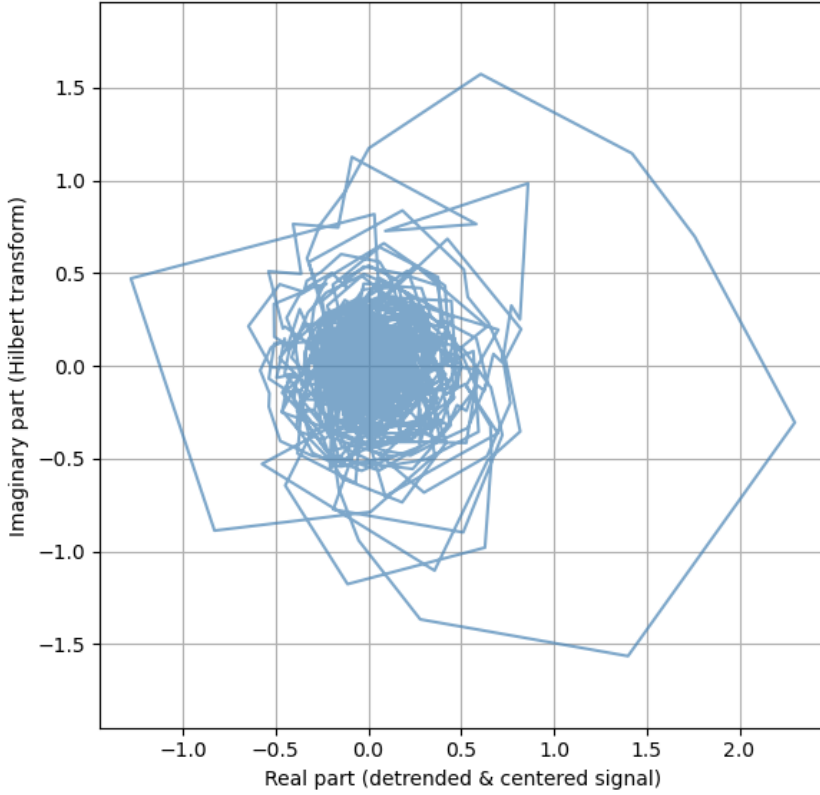


Figure 4: Complex Plane of Hilbert Transform (Temperature)

indicate transient transitions or perturbations, perhaps driven by environmental fluctuations or active regulatory events. Unlike ideal oscillating systems that produce closed elliptical trajectories, the lack of strong periodic or rotational structures in the phase diagram suggests that the temperature dynamics are quasi-steady-state and based primarily on fluctuations rather than intrinsic oscillations. Figure 5 shows that the system is primarily stable but responsive, with a clear regulatory target.

The phase diagram of the detrended honeycomb power signal shown in Figure 6 shows a compact elliptical cluster centered at the origin, with a structure similar to the temperature signal in Figure 4, but with a significantly wider distribution of amplitudes and rates of change. Unlike a purely periodic system with thin elliptical rings, the density and thickness of the clusters indicate a quasi-oscillatory but noisy behavior—possibly driven by internal switching mechanisms rather than smooth harmonic rhythms. The central concentration near zero still implies a steady-state equilibrium, but the wider dynamic range indicates that the system is more responsive and more actively regulated than the temperature system.

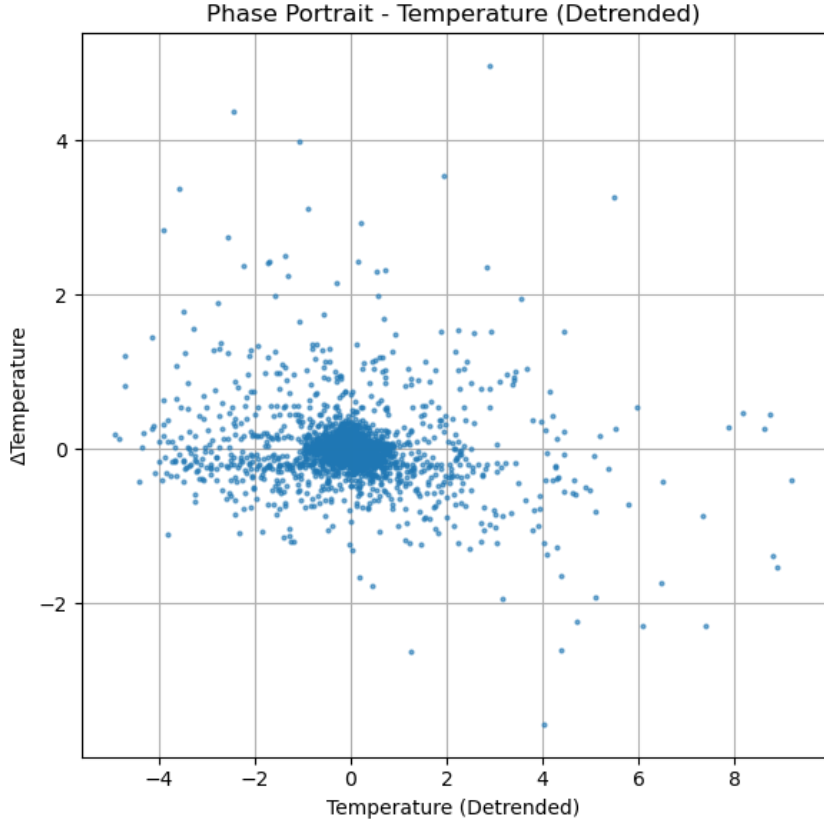


Figure 5: Phase Portrait - Temperature (Detrended)

3.3. Hilbert Analysis

To investigate the temporal patterns of the instantaneous frequency and phase of the signals, we applied the Hilbert transform to the temperature and power signals. This transform converts each real-valued signal into a complex analytic signal, from which the instantaneous phase and frequency can be derived. The instantaneous phase reflects the position of the signal oscillation at each instant and captures transient dynamics that may be missed by traditional amplitude-based analysis. The instantaneous frequency, derived from the time derivative of the phase, reveals how fast the signal phase changes, thus providing insight into the periodicity of thermal and energy dynamics. We performed this step of the analysis so that we could track the local temporal properties of the temperature and power modulations, such as how often they oscillate, when the mutations occur, and whether their timing is consistent. By using concentrated signals, we ensure that the assumptions of the Hilbert transform are met, making the extracted phase information more accurate and easier to interpret.

3.4. CRP and Coordination

To analyze the dynamic coordination between the temperature and power signals, we calculated the continuous relative phase (CRP) by subtracting the instantaneous phase

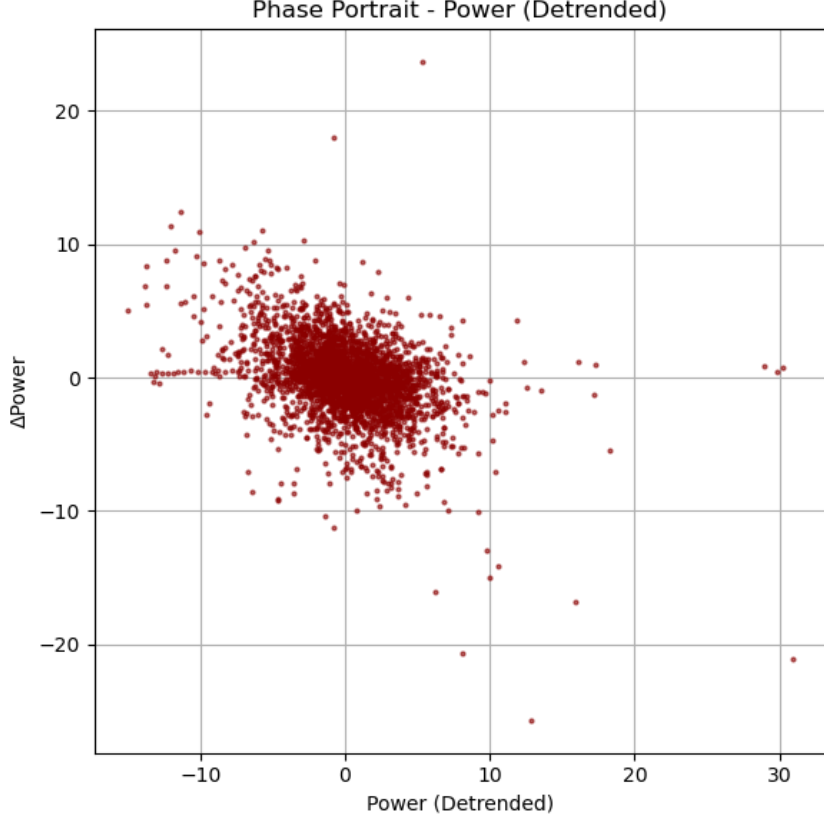


Figure 6: Phase Portrait - Power (Detrended)

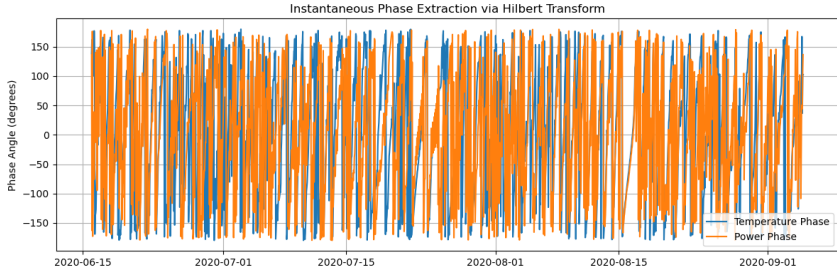


Figure 7: Instantaneous Phase Extraction via Hilbert Transform

of the power signal from the temperature signal. This allows us to observe how the two signals synchronize over time. By observing the temporal evolution of the instantaneous phase, we first confirm that both signals exhibit rhythmicity: temperature follows quasi-periodic environmental cycles, while power exhibits faster, often threshold-triggered phase shifts. These underlying rhythmic structures make the CRP estimates meaningful. During stable time intervals, CRP values are close to zero or $\pm 180^\circ$, indicating a consistent pattern of coordination. The periodicity of CRP fluctuations reflects unstable coupling or environmental perturbations.

To further quantify the pattern of coordination between the temperature and power signals, we computed several phase-based metrics. The vector strength of the CRP distribution is 0.578, indicating a moderate degree of phase locking, the signals show

clear synchronization, although not always perfectly aligned. The kurtosis of the CRP distribution is relatively low (0.80), indicating that the relative phase values are highly dispersed rather than narrowly concentrated around one value. This dispersion reflects adaptive coupling rather than strict entrainment.

We observe that the temperature signal leads the power signal in about 60.82 percent of the time samples and lags the power signal in 39.18 percent of the time samples. This asymmetry suggests that changes in temperature dynamics tend to drive subsequent changes in power, supporting the interpretation that the system responds to thermal fluctuations by delaying energetic regulation. Together, these findings suggest a goal-directed yet flexible coordination mechanism: the system remains partially synchronized to maintain homeostasis but allows for temporal changes to adapt to environmental and internal changes.

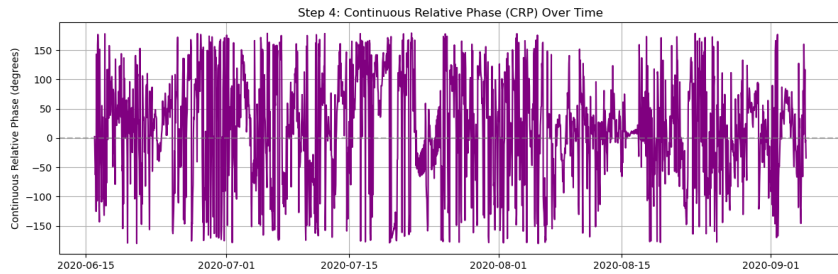


Figure 8: Continuous Relative Phase (CRP) Over Time

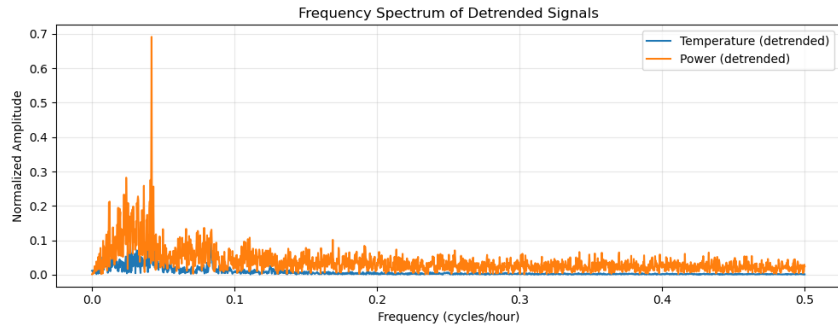


Figure 9: Frequency Spectrum of Detrended Signals

4. Discussion

This study uses a phase-based analytical perspective to explore five core questions about coordination. The interaction between temperature and power reveals a rhythmic coupling pattern. Specifically, the observed coordination model based on continuous relative phase (CRP) is dominated by in-phase dynamics, with occasional brief divergences. These findings are consistent with Kelso's model of coordination dynamics [2]. In this study,

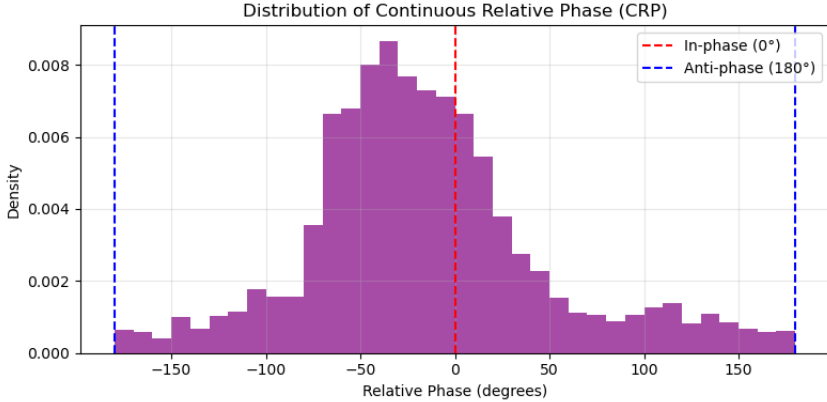


Figure 10: Distribution of Continuous Relative Phase (CRP)

we describe in-phase and anti phase states such that environmental or behavioral perturbations appear to induce changes around a central attractor, reflecting a flexible and goal-directed thermoregulatory strategy.

The moderate vector strength (0.578) indicates that the phase coupling is non random and highly adaptive, while the relatively low CRP kurtosis (0.80) reflects phase dispersion, indicating that the system does not operate under strict entrainment but is dynamically flexible. In addition, in 60.82 percent of the observations, temperature leads power, supporting a reactive regulatory mechanism that adaptively adjusts energy output based on thermal signals.

These results confirm the CRP analysis recommendations of Lamb and Stöckl (2014)[3], in particular regarding signal centering, Hilbert-based instantaneous phase extraction, and temporal filtering. In this context, the behavioral coordination of temperature and power reflects the adaptive intelligence of natural systems (e.g., honey bee colonies) and provides a theoretical basis for the design of robust and efficient environmental control systems..

Our results support Lamb and Stöckl's (2014)[3] suggestions for CRP analysis in practical systems, including appropriate centralization, Hilbert transform, and filtering. The results of this study explain the environmental regulation wisdom of the bee colony, which also provides a theoretical reference for many optimization designs. In the future, our research can further explore the system coordination mechanism under multi-parameter coupling and external disturbances.

5. Conclusion

This paper demonstrates the utility of CRP and Hilbert transform in analyzing the coordination between environmental (temperature) and functional (power) signals. Our results show that both signals show intrinsic rhythmicity and are mostly in phase, reflecting a high degree of temporal synchronization. The CRP dynamics show the changes

in attractor behavior over time. Its coordination is consistent with the principles of coordination dynamics theory. These tools provide new insights into the dynamic behavior of environmental systems and pave the way for future research in multivariable synchronization and control.

Through systematic research results, dynamic visualizations show that simple methods in complex system science - especially the treatment of phase partners in synchronization phase analysis, signal concentration and development phases - can be successfully applied to national-level data. These methods reveal the underlying dynamic structure and constitute an effective means to monitor the stability, switching and coordination of complex natural and engineered systems.

References

- [1] Emily A. Butler. Temporal interpersonal emotion systems: The “ties” that form relationships. *Personality and Social Psychology Review*, 15(4):367–393, 2011.
- [2] Hermann Haken, J. A. Scott Kelso, and H. Bunz. A theoretical model of phase transitions in human hand movements. *Biological Cybernetics*, 51(5):347–356, 1985.
- [3] Peter F. Lamb and Michael Stöckl. On the use of continuous relative phase: Review of current approaches and outline for a new standard. *Clinical Biomechanics*, 29(5):484–493, 2014.
- [4] M. Rosenblum and J. Kurths. Analyzing synchronization phenomena from bivariate data by means of the hilbert transform. In *Nonlinear Analysis of Physiological Data*, pages 91–99. Springer, 1998.

Dynamic Time Warping as an Alternative Pairwise Coordination Assessment

Novelty Addition to Entry 6 - Module 8

Group 6: Djourdan Johnson, Jacuqot Qiu, Lotte Michels, Nawat Nawati Azhati, Nuo Xu, Xuelin Wei

1 Measuring Pairwise Coordination

Analyzing coordination involves capturing the ways in which components of a system change together over time. There is a plethora of methods that can be employed to quantify such pairwise interactions (Cliff et al., 2023). One such method is the Hilbert transformation, that was demonstrated in the previous e-portfolio entry. Although this is a classical approach for pairwise coordination analysis, various recent papers point out that it can not account well for noise in a signal (Tao, 2024; Wodeyar et al., 2023). The MSPB dataset (Zhu et al., 2024) that is used in this project, however, may contain quite some noise, as found in the first entry of this e-portfolio.

With this in mind, we will further examine pairwise coordination in the beehive signals using a method that has not been covered in the Complex Systems course: Dynamic Time Warping (DTW). Originally proposed in 1978 by Sakoe and Chiba, DTW remains widely applied and actively researched across domains. Moreover, it has been proposed as a noise- and non-stationarity resistant approach compared to the Hilbert transformation (Tao, 2024). In this entry, we will briefly illustrate the underlying concept of DTW and demonstrate its applicability to the MSPB dataset.

The code used for the computations and visualizations in this entry can be found [here](#).

2 Background

DTW was designed to measure the similarity of two time-series based on their optimal alignment (Sakoe and Chiba, 1978). By first temporally matching two signals, the algorithm accounts for inter-signal differences regarding length, lag and phase. Thus, DTW can find pairwise interactions regardless of temporal incongruities, in contrast to traditional similarity metrics such as a straight-forward euclidian distance computation (Mishra, 2021).

The underlying notion of DTW is best explained using an exemplary visualization. All DTW outcomes and visualizations in this e-portfolio entry are generated using the dtw-python package (Giorgino, 2009). Figure 1 displays the alignment returned by the DTW algorithm for the raw beehive temperature and humidity time-series. The diagonal lines indicate the point-to-point mapping to match the signals in such a way that their cumulative distances are minimized.

DTW computes this minimization by setting up a 'cost matrix' and finding the 'cheapest' warping path through this matrix from the bottom left corner to the upper right corner.

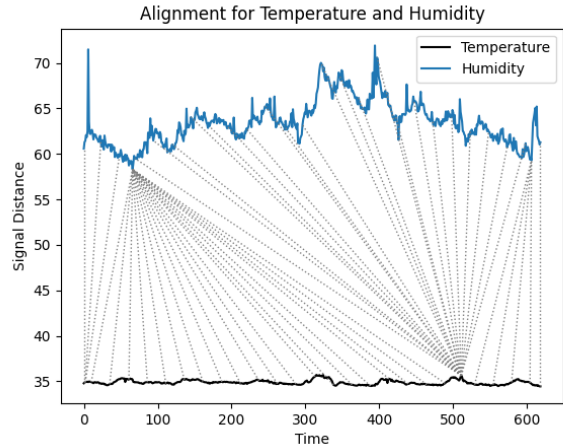


Figure 1: DTW alignment result between the raw temperature and humidity signals. For clarity purposes, the signals are displayed for one week of data (August 8 - August 14).

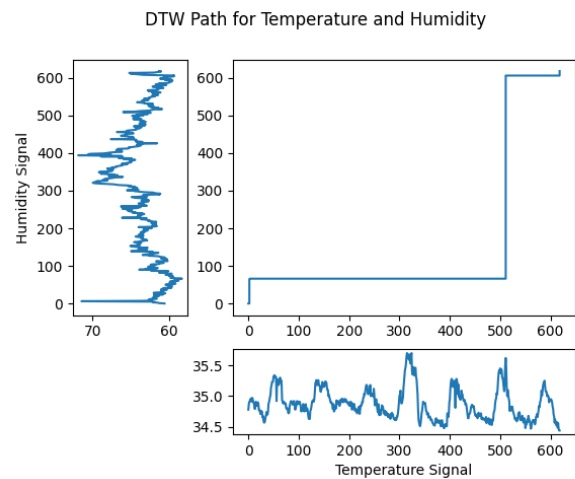


Figure 2: Warping path between the temperature (horizontal) and humidity (vertical) signals corresponding to Figure 1.

To give an example, the warping path corresponding to the alignment in Figure 1 is included in Figure 2.

Horizontal and vertical segments in a warping plot indicate one signal holding a value while the other progresses. Thus,

humidity holds a value while temperature progresses until around the 500th timepoint, after which these roles switch.

3 Pre-Processing Steps and Parameter Settings

Figure 1 highlights an important aspect of the MSPB dataset: the time-series are heterogeneous. Specifically, temperature is measured in degrees Celsius; humidity is measured in relative percentage; beehive activity is measured using Fourier transform power values. These different units exhibit varying means and standard deviations, as can be seen in Figure 1.

Rather than being dominated by such unit characteristics, coordination analyses should reflect only signal shape or temporal structure. As such, two important pre-processing steps need to be taken before DTW implementation: 1) similar to the preparations for the Hilbert transform seen previously, signals need to be centered around a zero mean and 2) signals need to be standardized. In our code, the StandardScaler function from the sklearn package is used (Pedregosa et al., 2011). This functionality performs both the centering and scaling steps to the inputted time-series.

Additionally, prior to applying DTW, it is important to consider constraints on the alignment path to ensure meaningful temporal correspondences. Figure 1 shows that some signal measurements are connected over a temporal lag of more than 400 timepoints, which represents over 4 days in the MSPB dataset (see the first e-portfolio entry for a dataset description). In the context of beehive research, it does not make sense to consider pairwise interactions between temperature, humidity and colony activity over such an extended time period (Zhu et al., 2024).

To restrict the temporal deviation between aligned time points, a windowing function can be applied. Conventionally, we apply a Sakoe-Chiba window (Sakoe and Chiba, 1978). This functionality can be used to define a fixed bandwidth around the diagonal of the cost matrix within which the warping path must lie. This bandwidth is determined by the window size parameter. We set this parameter to 48 timepoints to avoid alignments connected over more than half a day in time, which is a more intuitive timespan in the context of beehives (Zhu et al., 2024).

Figures 3 and 4 show the DTW results for the temperature and humidity signals after these pre-processing and parameter setting steps.

4 Dynamic Time Warping Results

After determining the pre-processing steps and parameter settings, the DTW algorithm was applied on the complete time-series from the MSPB dataset in a pairwise fashion: temperature against humidity, power against humidity, and temperature against power. The warping results are displayed in Figure 5.

Based on these alignments, the distance between two signals can be computed. The distance feature returned by the dtw-python package is the accumulation of the euclidean distances between the matched signal points (Giorgino, 2009). This can be normalized by dividing by the length of the signals, which results in an average distance between two signals.

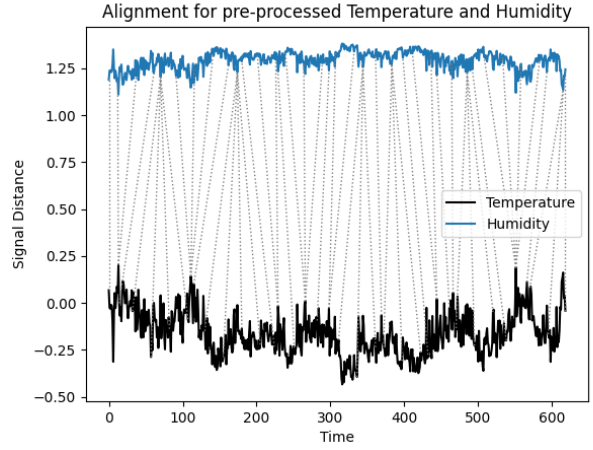


Figure 3: Sakoe-Chiba DTW alignment result between the pre-processed temperature and humidity signals. Matching Figure 1, the signals are displayed for one week of data (August 8 - August 14).

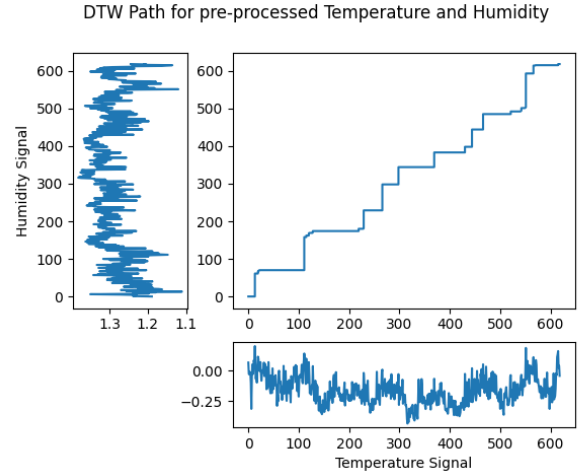


Figure 4: Sakoe-Chiba DTW warping path between the pre-processed temperature (horizontal) and humidity (vertical) signals corresponding to Figure 3.

Normalized distance is 1.25 for the temperature-humidity alignment, 2.33 for the power-humidity alignment and 0.96 for the temperature-power alignment. Out of the three pairwise comparisons, the temperature and power signals thus seem to be most correlated.

However, it is hard to interpret a degree of similarity or coordination based merely on the distance metric. Lower distance values indicate better alignment, but there's no inherent threshold for what counts as "similar" or "coordinated" as the meaning of distance values is often context-dependent.

Some solutions have been proposed to get a better sense of signal coordination based on DTW outcomes. For instance, Stent (2024) described that an interpretable similarity score could be computed by dividing the cumulative distances by

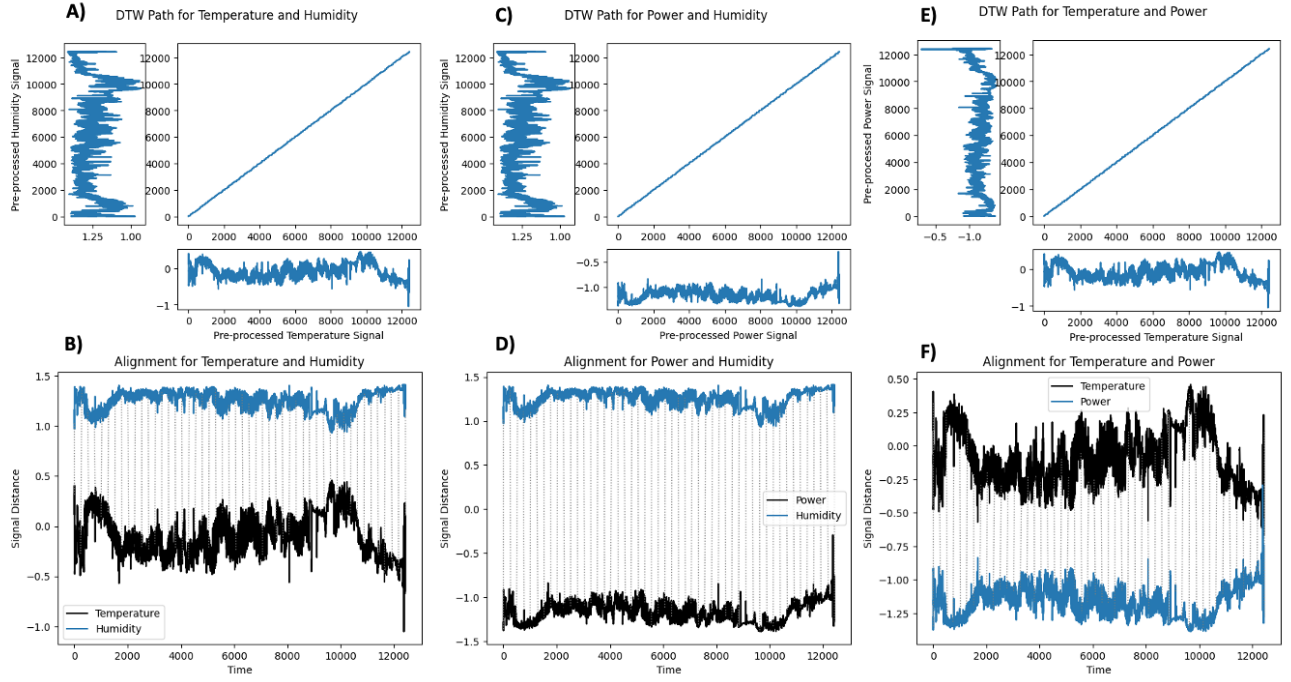


Figure 5: DTW Results for the full temporal signals in the MSPB dataset. A-B: Alignment for temperature and humidity, C-D: Alignment for power and humidity, E-F: Alignment for temperature and power.

the length of the best warping path found by DTW. The resulting metric will lie between 0 (identical signals) and 1 (no similarities were found at all). Applied to the beehive DTW alignments, this approach returns similarity scores of 0.01, 0.02 and 0.01 respectively. These DTW similarity scores thus indicate very high pairwise interactions within the beehive.

Stent (2024) does give a disclaimer, however, that these similarity metrics may be very informative by themselves, but should be considered alongside the graphical representations above (graphs B, D and F within Figure 5). These indeed do indicate some signal interactions, but stating the signals are structurally near to identical may be a far stretch, especially in plots B and F.

The bottom plots in Figure 5 also display another interesting aspect of the beehive time-series, namely that their relative distances and interactions may differ over time. This highlights another pitfall of the global distance or similarity metrics discussed so far: these measures assume stationary coordination over time. However, in many complex systems, pairwise interactions are not stationary. Examining coordination over time may thus be more informative than computing a single, aggregate statistic.

This issue is increasingly being addressed, for instance by Likens and Wiltshire (2020). These authors argue for the use of windowed analysis methods, in their case applied to multiscale synchrony. However, sliding windows can also be applied in conjunction with DTW (Linke et al., 2020; Meszlényi et al., 2017). The next section will therefore provide a more fine-grained pairwise coordination assessment, applying windowed DTW to explore pairwise interactions over time.

5 Windowed Dynamic Time Warping Results

In windowed DTW, a temporal window is slid over the time-series in a step-wise fashion. The DTW algorithm is applied at each step on the signal parts that fall within the window, returning a warping path and (normalized) distance metric for only that specific segment of the time-series. Thus, a sequence of distance values is obtained that can illustrate how pairwise interactions between two signals change over time.

This approach has been successfully applied in previous research, for instance by Linke et al. (2020). Their experiment involved windowed DTW to recognize functional connectivity anomalies in autistic subjects, outperforming other traditional pairwise interaction methods (such as Pearson correlation). Specifically, the authors used the windowed DTW distance values to retrieve signal similarity scores over time, following a computational approach proposed by Meszlényi et al. (2017). This approach entails that the sequence of distance values are multiplied by -1 and subsequently centered around zero. Next, it is proposed that resulting scores lower than zero indicate 'below average similarity' and resulting scores higher than zero indicate 'above average similarity'.

Following these guidelines, we applied windowed DTW to the time-series in the MSPB dataset. We created a temporal window of 96 timepoints, covering one day in the data; We made the informed assumption that the pairwise interactions between the beehive signals remained stationary over the time-course of one day (Zhu et al., 2024). Next, the DTW window was slid it over the temperature, humidity and power signals with a step size of one timepoint. At each step, DTW was implemented as delineated in the previous entry sections. Finally, following the guidelines by Meszlényi et al. (2017), the

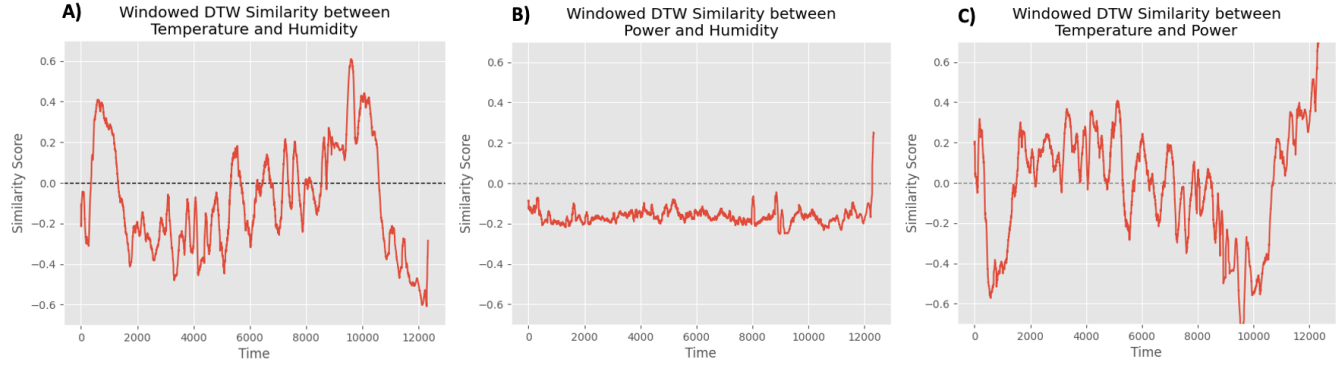


Figure 6: Signal similarity scores over time, obtained by Windowed DTW. Values above zero (dotted baseline) reflect 'above average' similarity. A: pairwise interactions over time between temperature and humidity, B: pairwise interactions over time between power and humidity, C: pairwise interactions over time between temperature and power.

obtained sequence of normalized distance scores were negated and demeaned. The resulting similarity scores over time are presented in Figure 6.

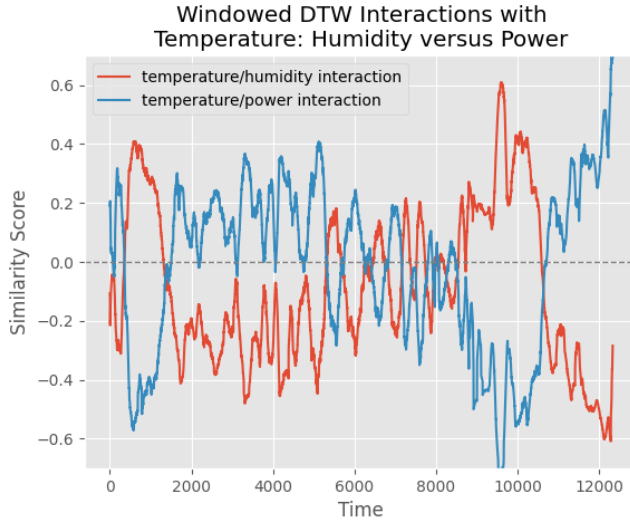


Figure 7: A combined plot of the windowed DTW similarity signals for both the temperature-humidity and temperature-power interactions.

The graphs in Figure 6 suggest that pairwise interactions change over time. Whereas the plots suggest no notable similarities between power and humidity, pairwise interactions seem to fluctuate for the temperature signal a lot more. The temperature-humidity and temperature-power pairings sometimes reach similarity scores of around 0.4, which indicates note-worthy coordination between these signals.

Interestingly, the windowed similarity scores for temperature-humidity and temperature-power seem to alternate over time. This becomes more clear in Figure 7. The fact that these similarity curves alternate over time suggests dynamic shifts in coordination between temperature and the two other variables.

These dynamic shifts may be interpreted within the context

of seasonal activities within honeybee colonies, as described by the Mid-Atlantic Apiculture Research and Extension Consortium (2010). Transitioning into the summer or winter period, beehives show emergent thermo-moisture regulators which keeps the temperature within the beehive more or less around 33 degrees Celsius, which is best for brooding. These transition periods are visible in the large red peaks in Figure 7. For instance, the peak around timepoint 10,000 represents the months of September and October, during which honeybees will form a tight cluster to maintain core temperature in their hive (Research and Consortium, 2010). Colony activity may then be low, while humidity and temperature inside the hive are more tightly coupled due to condensation from respiration and minimal hive fanning behavior.

In contrast, during the summer period (in between timepoints 2000 to 6000), honeybees show active foraging behavior including the gathering of water for the regulation of beehive temperature (Research and Consortium, 2010). This active thermoregulation is thus reflected in an increase in pairwise interaction between colony temperature and power, visible by the blue peaks in Figure 7. This phenomenon was also discovered when investigating the cross-recurrence between temperature and hive power in entries 4 and 5 (on modules 6 and 7).

Lastly, before committing to these findings, surrogate tests were conducted to assess the robustness of the DTW similarity results and preclude any spurious outcomes. The applied surrogate testing methods are described in more detail in Entry 5/Module 7 of this ePortfolio. The surrogate test results are displayed in Figure 8. First, data shuffling was applied and repeated 20 times. The windowed DTW results on the surrogate signals show no significant pairwise interactions. In addition, segment shuffling was applied. Segments of 24 hours were created to maintain the daily cycles typically displayed by honeybeehive time-series as seen in Entry 1/Module 2 and described by Zhu et al. (2024). Again, segment shuffling was repeated 20 times and no significant pairwise interactions came up. Thus, both surrogate tests indicate that the findings from windowed DTW in Figure 6 and 7 are robust.

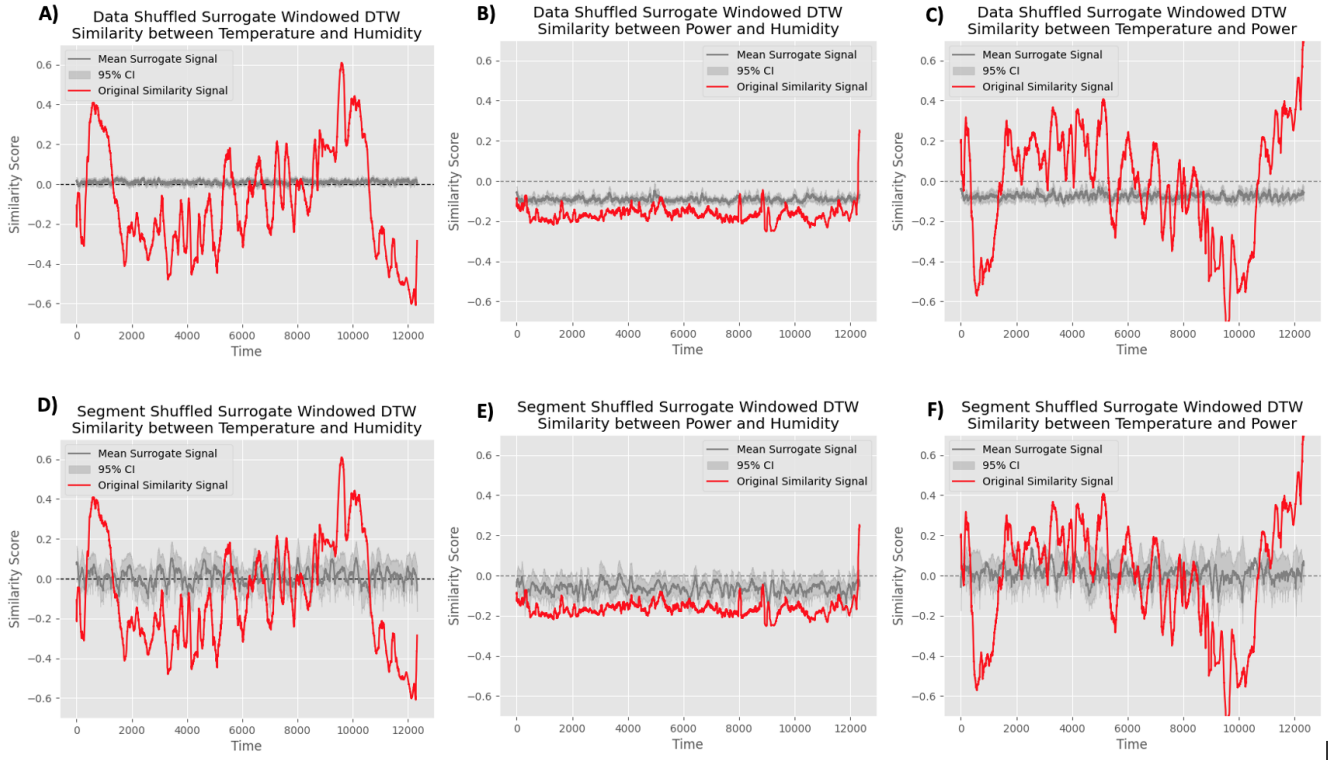


Figure 8: Surrogate test results on the windowed DTW findings. The gray markers indicate the mean and 95% confidence interval after 20 rehearsals. The original temperature-humidity and temperature-power interactions are significantly different from the surrogate distributions (graphs A-D and C-F).

6 Conclusion

To summarize, Dynamic Time Warping (DTW) can be applied as a noise- and non-stationarity resistant approach towards pairwise coordination analysis. DTW can be used to align signals of different units, given that these signals are centered and scaled. Moreover, for DTW to make meaningful alignments between two sequences, it is important set a contextually relevant point-to-point matching bandwidth. DTW can then be used to obtain an aggregate signal distance and signal similarity score. However, these metrics are very much context-dependent, making them hard to interpret, and do not take temporal coordination variations into account. We demonstrated that windowed DTW may be a more suitable approach towards examining the pairwise coordination over time in complex systems such as a beehive. For the beehive that is investigated throughout our ePortofolio, notable pairwise coordinations for the temperature-humidity and temperature-power alignments were found. Interestingly, these interactions alternated each other, indicating dynamic coordination shifts in the beehive over time. These dynamic shifts may reflect typical seasonal behaviors shown by honeybees over the year. Surrogate tests confirmed the robustness of these findings.

References

[Cliff et al.2023] Oliver M. Cliff, Annie G. Bryant, Joseph T. Lizier, Naotsugu Tsuchiya, and Ben D. Fulcher. 2023. Uni-

fying pairwise interactions in complex dynamics. *Nature Computational Science*, 3(10):883–893, 9.

[Giorgino2009] Toni Giorgino. 2009. Computing and Visualizing Dynamic Time Warping Alignments in R: The dtw Package. *DOAJ (DOAJ: Directory of Open Access Journals)*, 8.

[Likens and Wiltshire2020] Aaron D Likens and Travis J Wiltshire. 2020. Windowed multiscale synchrony: modeling time-varying and scale-localized interpersonal coordination dynamics. *Social Cognitive and Affective Neuroscience*, 16(1-2):232–245, 9.

[Linke et al.2020] A.C. Linke, L.E. Mash, C.H. Fong, M.K. Kinnear, J.S. Kohli, M. Wilkinson, R. Tung, R.J. Jao Keehn, R.A. Carper, I. Fishman, and R.-A. Müller. 2020. Dynamic time warping outperforms Pearson correlation in detecting atypical functional connectivity in autism spectrum disorders. *NeuroImage*, 223:117383, 9.

[Meszlényi et al.2017] Regina J. Meszlényi, Petra Hermann, Krisztián Buza, Viktor Gál, and Zoltán Vidnyánszky. 2017. Resting State fMRI Functional Connectivity Analysis using dynamic time warping. *Frontiers in Neuroscience*, 11, 2.

[Mishra2021] Abhishek Mishra. 2021. Time series similarity using dynamic time warping -Explained. 12.

[Pedregosa et al.2011] F. Pedregosa, G. Varoquaux, A. Gramfort, V. Michel, B. Thirion, O. Grisel, M. Blondel, P. Prettenhofer, R. Weiss, V. Dubourg, J. Vanderplas, A. Passos, D. Cournapeau, M. Brucher, M. Perrot, and E. Duchesnay.

2011. Scikit-learn: Machine learning in Python. *Journal of Machine Learning Research*, 12:2825–2830.

[Research and Consortium2010] Mid-Atlantic Apiculture Research and Extension Consortium. 2010. Seasonal Cycles of Activities in Colonies, 6.

[Sakoe and Chiba1978] H. Sakoe and S. Chiba. 1978. Dynamic programming algorithm optimization for spoken word recognition. *IEEE Transactions on Acoustics Speech and Signal Processing*, 26(1):43–49, 2.

[Stent2024] Mark Stent. 2024. Dynamic Time Warping - Mark Stent - Medium. 11.

[Tao2024] Xiyue Tao. 2024. Dynamic time warping based instantaneous frequency estimation for rotating machineries under non-stationary operating conditions. *Journal of Physics Conference Series*, 2815(1):012044, 8.

[Wodeyar et al.2023] Anirudh Wodeyar, Francois A Marshall, Catherine J Chu, Uri T Eden, and Mark A Kramer. 2023. Different methods to estimate the phase of neural rhythms agree, but only during times of low uncertainty. *bioRxiv (Cold Spring Harbor Laboratory)*, 1.

[Zhu et al.2024] Yi Zhu, Mahsa Abdollahi, Ségolène Maucourt, Nico Coallier, Heitor R. Guimarães, Pierre Giovenazzo, and Tiago H. Falk. 2024. MSPB: a longitudinal multi-sensor dataset with phenotypic trait measurements from honey bees. *Scientific Data*, 11(1), 8.

Empirical Dynamic Modeling of Beehive Coordination Dynamics

Djourdan Gomes-Johnson

TiU CSAI / snr: 2033032

d.a.e.d.s.g.johnson@tilburguniversity.edu

Abstract

This study investigates the internal dynamics of a sensor-instrumented beehive by applying empirical dynamic modeling (EDM) to high-resolution time series data. Focusing on three key signals: hive power, humidity, and temperature, this analysis assesses intrinsic predictability, nonlinearity, and potential causal relationships. Using a combination of Simplex projection, sequential locally weighted global linear maps (S-Map), Convergent Cross Mapping (CCM), and multiview embedding, the study reveals distinct dynamic roles for each signal. Hive power exhibited strong internal regularity ($\rho = 0.993$), consistent with its role as a proxy for colony-level metabolic activity. Humidity, by contrast, demonstrated lower self-predictability ($\rho = 0.63$) and showed only a modest, variable dependence on hive power ($\rho = 0.66$), suggesting that it is more susceptible to external environmental influences and less governed by internal colony dynamics. Temperature dynamics were internally predictable ($p = 0.991$), but contributed minimally to predicting hive power. Multiview embedding consistently improved forecasting skill across variables. These results highlight the utility of EDM in uncovering asymmetrical coupling, attractor behavior, and internal regulation within biological systems, providing new insights into the coordination strategies of beehives.

Keywords: EDM, Honeybee Sensor Data, Nonlinear Time Series Analysis

1 Introduction

Bee colonies represent paradigmatic examples of complex biological systems, where environmental regulation and collective behavior emerge through decentralized coordination (Camazine et al., 2001). Within this dynamic framework, hive power serves as a macroscopic proxy for

colony-level metabolic output, encompassing both thermoregulatory and communicative processes (Bencsik et al., 2011). In parallel, environmental conditions such as humidity and micro-vibrational patterns provide windows into both external perturbations and internal response dynamics (Meikle et al., 2015), (Ramsey et al., 2020).

Recent advances in sensor technology have enabled continuous monitoring of beehive environments, offering high-resolution time series data of mechanical and environmental variables (Wario et al., 2015). While traditional time series methods often assume stationarity or linear dependence, such assumptions fall short in capturing the intrinsic nonlinearity and time-varying nature of biological coordination (Sugihara et al., 2012). Addressing this gap, this study applies tools from empirical dynamic modeling (EDM)—a framework rooted in state space reconstruction and attractor-based analysis—to investigate the coupling and causal structure between hive power, humidity, and vibrational signals.

Building on previous studies that utilized phase-based analyses (e.g., Hilbert transform and continuous relative phase) to characterize coordination in environmental signals (Lamb and Stöckl, 2014), we adopt an alternative yet complementary approach that reconstructs system behavior directly from observed time series data. The primary goals are twofold: (1) to assess the intrinsic predictability and complexity of humidity and vibrational signals, and (2) to evaluate the dynamic influence of hive power on these variables. In doing so, this paper aims to uncover signal interdependencies that reveal the structure and coordination mechanisms underpinning beehive dynamics.

2 Methods

2.1 Dataset and Variables

This study utilized the `D1_sensor_data` dataset, comprising approximately 960,809 time-stamped observations collected from sensor-instrumented beehives. The dataset includes more than 30 variables representing environmental conditions and internal hive metrics. The analysis focused on four key variables:

`hive_power` serves as a proxy for colony-level

metabolic activity and thermoregulatory output, while `humidity` reflects the internal microclimate critical for brood development and colony homeostasis. `temperature` captures external or ambient thermal influence, contributing to assessments of regulatory feedback mechanisms.

2.2 Preprocessing

To ensure comparability across variables and prepare the data for empirical dynamic modeling, all time series were normalized using z-score transformation:

$$\text{Normalized Value} = \frac{\text{Value} - \mu}{\sigma}$$

where μ and σ represent the mean and standard deviation of each variable. The following normalized signals were used throughout the analysis: `hive_power_norm`, `humidity_norm`, and `temperature_norm`. A contiguous 1000-observation subset (rows 10,000 to 11,000) was extracted from the full dataset to ensure computational feasibility and facilitate detailed state-space exploration. The selected window contained no missing values.

2.3 Empirical Dynamic Modeling (EDM)

Empirical dynamic modeling (EDM) techniques, implemented via the `rEDM` package in R, were used to reconstruct underlying system dynamics and evaluate inter-variable dependencies. EDM reconstructs attractor manifolds using time-delay embeddings and does not rely on parametric assumptions, making it suitable for nonlinear ecological systems (?).

2.3.1 Simplex Projection

Simplex projection was used to evaluate the intrinsic predictability of each individual time series. Using lagged coordinates, embedding dimensions E were varied from 2 to 8. Each configuration was assessed by computing the Pearson correlation coefficient (ρ), mean absolute error (MAE), and root mean square error (RMSE) between predicted and observed values. The dataset was divided into a training library (observations 1–500) and a prediction interval (observations 501–1000). The optimal embedding dimension was determined by the E value that maximized ρ .

2.3.2 S-Map Analysis

The S-Map (sequential locally weighted global linear map) algorithm was applied to examine system nonlinearity and estimate time-varying interaction strengths. S-Map fits locally linear approximations across the reconstructed manifold, modulated by the nonlinearity parameter θ . Values of θ were tested from 0.0 to 2.0 in increments of 0.1.

Two modeling configurations were implemented: (1) univariate S-Map, where predictions for each variable were based solely on its own lagged history; and (2) multivariate S-Map, which incorporated `hive_power_norm` as an additional input to assess its causal influence. Coefficients derived from S-Map regressions were interpreted as time-varying partial derivatives, offering insight into the dynamic influence of hive power on target variables such as humidity and vibration.

2.4 Model Evaluation and Software/Tools

Model performance was evaluated using standard forecast diagnostics (p , MAE, RMSE). Visualization, conducted using the `ggplot2` package, included time series plots comparing observed and predicted values, p curves across embedding dimensions (Simplex), forecast accuracy across nonlinearity values θ (S-Map), and temporal trajectories of S-Map coefficients reflecting interaction strength and variability.

All computations were performed in R using the following libraries: `rEDM`, `tidyverse`, `ggplot2`, and `Kendall`.

3 Results

3.1 Dataset Overview

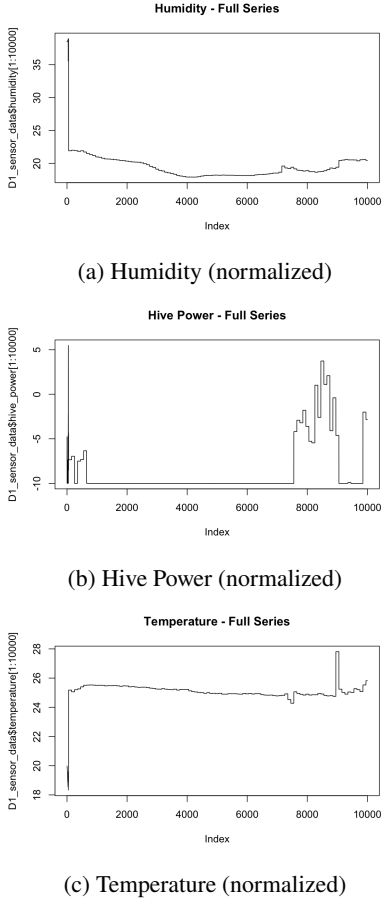


Figure 1: Normalized time series data for key internal and environmental signals.

The `D1_sensor_data` dataset consists of 960,809 rows of time-stamped measurements from instrumented bee-hives. Recorded metrics include hive activity (e.g., `hive_power`), and environmental parameters (e.g., `temperature`, `humidity`). A subset of 1,000 consecutive, complete observations was selected for analysis following normalization.

3.2 Univariate Predictability: Humidity

Intrinsic predictability of the `humidity_norm` signal was evaluated using Simplex projection. Forecasting accuracy peaked at embedding dimension $E = 6$ with a Pearson correlation coefficient of $p = 0.63$, mean absolute error (MAE) of 0.148, and root mean square error (RMSE) of 0.183. These values indicate moderate self-predictability, likely reflecting both internal regulation and influence from unmeasured environmental drivers.

Further evaluation with univariate S-Map revealed only a slight gain in forecasting skill across nonlinearity parameters, with a maximum $p = 0.64$ near $\theta = 0.5$. This weak response to varying θ suggests limited nonlinear structure and supports the interpretation of externally modulated or smooth, near-linear dynamics.

3.3 Univariate Predictability: Temperature

The `temperature_norm` signal exhibited strong deterministic structure under Simplex projection. The optimal embedding dimension was $E = 6$, producing $p = 0.991$, MAE of 0.035, and RMSE of 0.046. These results indicate highly regular behavior, consistent with gradual environmental variation or internally buffered thermoregulation.

Minimal gains were observed in the S-Map framework across the θ spectrum, confirming linearity and predictability of the temperature series. Lack of significant change in accuracy reinforces the interpretation of temperature as a stable and slow-moving variable.

3.4 Univariate Predictability: Hive Power

The `hive_power_norm` time series demonstrated high self-predictability, with optimal performance at $E = 6$, where $p = 0.993$, MAE = 0.039, and RMSE = 0.053. These metrics reflect a deterministic and internally regulated signal, suggesting consistent colony-level activity.

S-Map analysis showed marginal improvement with increased nonlinearity, peaking at $\theta \approx 0.9$ with $p = 0.994$. This indicates weak but present nonlinear dynamics, possibly associated with adaptive metabolic responses or behavioral variability.

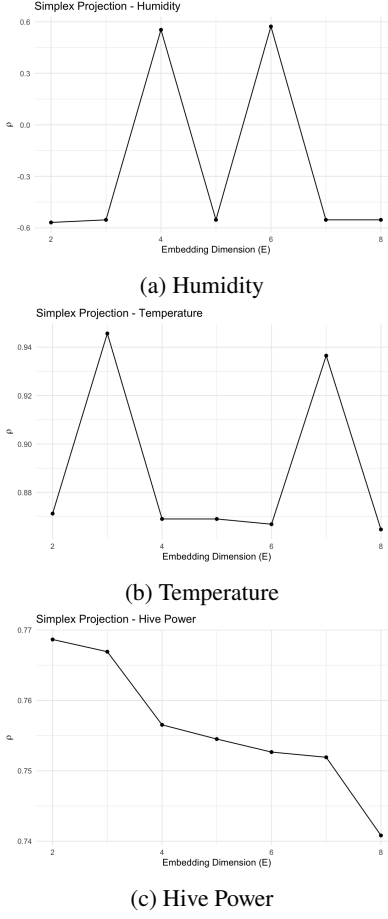


Figure 2: Simplex projection accuracy across embedding dimensions (E) for key variables.

3.5 Multivariate S-Map: Hive Power as a Driver

Multivariate S-Map was used to assess the dynamic influence of `hive_power_norm` on other signals. When hive power served as the target variable, predictive skill improved to $p = 0.995$ at $E = 6$ and $\theta = 0.9$, outperforming the univariate baseline. Time-varying coefficients $\partial\text{Vibration}/\partial\text{HivePower}$ were consistently positive and stable, suggesting a robust influence of hive power on vibrational output.

For `humidity`, the addition of `hive_power` as a predictor led to a marginal improvement in forecasting ($p = 0.66$), accompanied by fluctuating coefficient trajectories, indicative of weaker or conditional dependence.

3.6 Temperature–Hive Power Interactions

To examine whether temperature dynamically influenced hive power, a multivariate S-Map was conducted. Predictive skill increased only marginally ($p = 0.994$ vs. $p = 0.993$ in the univariate case), while estimated coefficients $\partial\text{HivePower}/\partial\text{Temperature}$ remained close to zero throughout. These findings imply minimal dynamic

coupling, reinforcing the interpretation that hive power may regulate temperature, rather than being directly influenced by it.

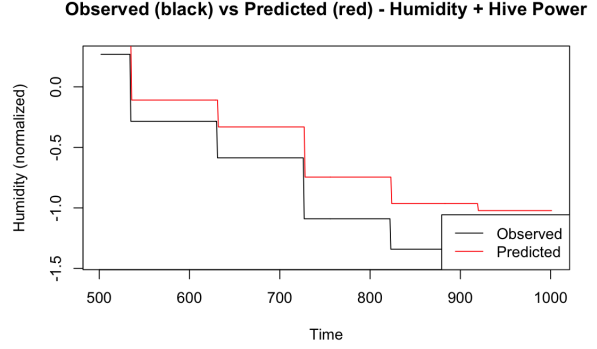


Figure 3: Observed vs. predicted humidity using multivariate S-Map with hive power as input.

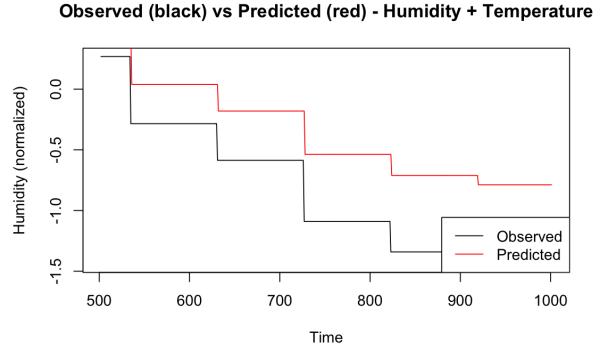


Figure 4: Observed vs. predicted humidity using temperature as input.

3.7 Causal Discovery via Convergent Cross Mapping (CCM)

CCM analysis revealed the strongest causal influence from `hive_power` to `vibration`, with cross-map skill increasing steadily with library size. In contrast, the relationship between `hive_power` and `humidity` appeared bidirectional but weak, with only slight asymmetry in predictive skill. No significant causal influence was detected from temperature to hive power, as evidenced by flat CCM convergence curves.

3.8 Multiview Embedding

Application of Multiview embedding improved forecasting robustness across all variables. The method achieved $p = 0.994$ for `hive_power`, indicating that ensemble embedding approaches effectively synthesize multiple perspectives of the underlying dynamics.

3.9 Time-Varying Interaction Strengths

Temporal profiles of interaction strength, as inferred from S-Map coefficients, demonstrated that:

- Hive power exerted a consistently positive and stable influence on vibration.
- Hive power's influence on humidity was weak and fluctuating.
- Temperature showed minimal influence on hive power, with noisy and near-zero coefficient values.

These observations support a causal hierarchy wherein hive power acts as a central modulator of internal hive signals, while external factors such as temperature play more constrained or indirect roles.

4 Discussion and Conclusion

4.1 Summary of Findings

This study employed empirical dynamic modeling (EDM)—including Simplex projection, S-Map analysis, Convergent Cross Mapping (CCM), and Multiview embedding—to examine the internal dynamics of a sensor-instrumented beehive. The `humidity_norm` signal demonstrated moderate self-predictability, with a correlation coefficient of approximately $\rho = 0.63$. This suggests that humidity is influenced by both endogenous hive factors and exogenous environmental conditions. The S-Map analysis revealed minimal nonlinear structure in the humidity signal, indicating relatively smooth or linear dynamics. The inclusion of `hive_power` as a covariate in multivariate S-Map models improved prediction of dynamics to $\rho \approx 0.995$, with consistently positive interaction coefficients.

Temperature showed negligible dynamic influence on hive power. Both multivariate S-Map and CCM analyses yielded coefficients near zero and non-converging causal curves, reinforcing the hypothesis that hive power governs internal temperature regulation, rather than responding to it. Among all techniques applied, multiview embedding achieved the highest predictive accuracy, with $\rho > 0.995$ for `hive_power`, underscoring the utility of ensemble embeddings in noisy, nonlinear biological systems.

4.2 Interpretation

These findings reveal a hierarchical organization in beehive dynamics, where internal metabolic activity—as proxied by `hive_power`—plays a central role in driving collective vibrational behavior. Humidity and temperature exhibit weaker and less consistent associations with hive power, consistent with the biological understanding that bees actively regulate their internal environment and

buffer external fluctuations. Overall, these results highlight the capacity of EDM to uncover structured, non-linear dependencies that characterize complex adaptive systems such as honeybee colonies.

4.3 Limitations and Future Work

This analysis was constrained by a limited selection of variables and a short observation window. While the focus on hive power, humidity, and temperature provided meaningful insights, future work should incorporate additional ecological drivers. Furthermore, the analysis was conducted on a 1000-row subset of the full dataset for computational tractability. Extending these methods to longer time windows or seasonal timescales could reveal slower dynamics, including regime shifts or adaptive transitions in colony behavior.

References

- M. Bencsik, M. Baxter, A. Lucian, J. Romieu, and M. Millet. 2011. Honeybee colony vibration monitoring using accelerometers. *Sensors*, 11(5):4788–4806.
- Scott Camazine, Jean-Louis Deneubourg, Nigel R. Franks, James Sneyd, Guy Theraulaz, and Eric Bonabeau. 2001. *Self-Organization in Biological Systems*. Princeton University Press.
- Peter F Lamb and Michael Stöckl. 2014. On the use of continuous relative phase: Review of current approaches and outline for a new standard. *Clinical Biomechanics*, 29(5):484–493.
- William G Meikle, Martin Weiss, and Andrew R Stillwell. 2015. Using within-day hive weight changes to measure environmental effects on honey bee colonies. *PLOS ONE*, 10(8):e0134216.
- Samuel D Ramsey, Ronald Ochoa, Gary Bauchan, Christine Gulbranson, James D Mowery, Arnold Cohen, Daniel Lim, Josh Joklik, Joseph M Cicero, and James D Ellis. 2020. Mechanical and genetic pathways of resistance to varroa destructor in honey bees. *Nature Communications*, 10(1):1–13.
- George Sugihara, Robert May, Hao Ye, Chih-hao Hsieh, Ethan Deyle, Michael Fogarty, and Stephan Munch. 2012. Detecting causality in complex ecosystems. *Science*, 338(6106):496–500.
- Fidelis Wario, Bernd Wild, Raúl Rojas, and Tim Landgraf. 2015. Automatic detection of bee colony activity using video and sound data. *arXiv preprint arXiv:1504.00271*.

System Complexity and Information Theory (Entropy)

Entry 8 - Module 12

Group 6: Djourdan Johnson, Jacuqot Qiu, Lotte Michels, Nawat Nawati Azhati, Nuo Xu, Xuelin Wei

1 Introduction

Honey bee colonies (*Apis mellifera*) are essential for global food production, yet face threats from climate change and parasitic mites [1]. Non-invasive, sensor-based monitoring provides a promising way to assess hive health dynamically [2]. In this study, we analyze Hive 202204 using data from the MSPB dataset [3], which includes temperature, humidity, and audio-derived hive power measures. We focus on three entropy metrics—Shannon Entropy, Approximate Entropy (ApEn), and Sample Entropy (SampEn)—to quantify the complexity and predictability of hive dynamics. Our goal is to identify seasonal trends from April to November 2020, with particular attention to hive power as an indicator of bee activity. We also compare our findings to previously reported seasonal behavior patterns in the full MSPB cohort. By combining entropy metrics with time series and transfer entropy analyses, we aim to evaluate the sensitivity of each method in capturing dynamic shifts in colony behavior.

The code used for the computations and visualizations in this entry can be found [here](#).

2 Data Preprocessing

To conduct entropy and information flow analysis, we preprocessed the D1_sensor.csv file from the MSPB dataset. This file contains approximately 960,809 records, spanning from April 16 to November 5, 2020. We first filtered the data to include only records from hive 202204 and retained key columns (published_at, temperature, humidity, hive_power, and tag_number). To ensure temporal uniqueness of the time series, we removed duplicate timestamps. The time series was then aggregated to hourly averages, sorted chronologically, and grouped by month to enable monthly analyses.

Building on this, we further cleaned the data to meet the requirements for transfer entropy analysis. Specifically, we removed any records that contained missing values in the three main variables: temperature, humidity, or hive_power. This resulted in a clean, hourly-sampled dataset consisting of 3,209 records covering the main summer and early autumn months. We visualized missingness using a missingno matrix to confirm that the working dataset was complete. Monthly counts confirmed sufficient data coverage from June to October 2020, while May and November were excluded from the *transfer entropy* and *characteristic time scale* analyses due to an insufficient number of hourly records (fewer than 30).

3 3. Shannon Entropy ApEn and SampEn Analysis

Entropy measures were computed for temperature, humidity, and hive power using R, with parameters $m = 2$, $r = 0.2 * \text{SD}$ for ApEn and SampEn, and 10 bins for Shannon Entropy [4]. Results were aggregated monthly and visualized as line plots.

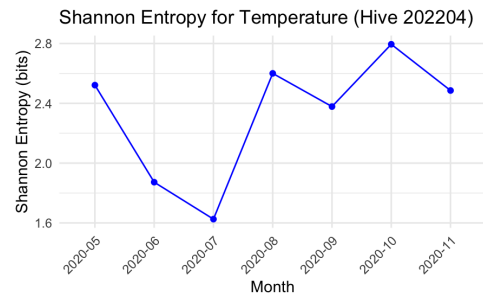


Figure 1: Shannon Entropy for Temperature

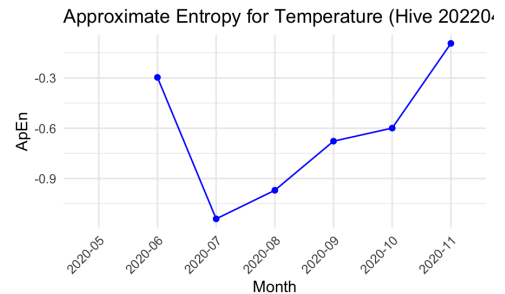


Figure 2: Approximate Entropy for Temperature

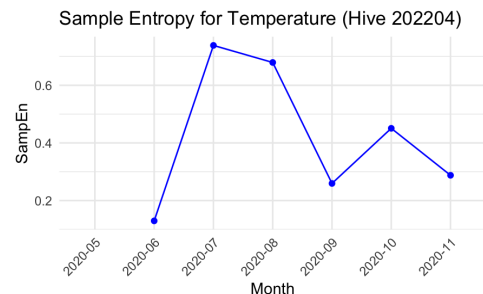


Figure 3: Sample Entropy for Temperature

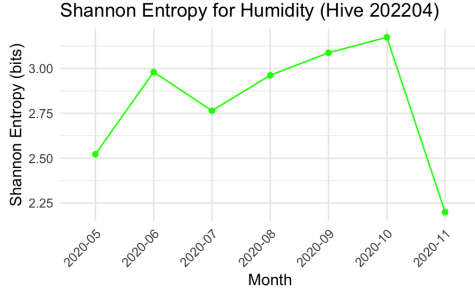


Figure 4: Shannon Entropy for Humidity

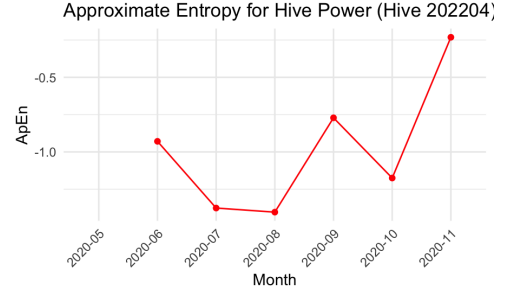


Figure 8: Approximate Entropy for Hive Power

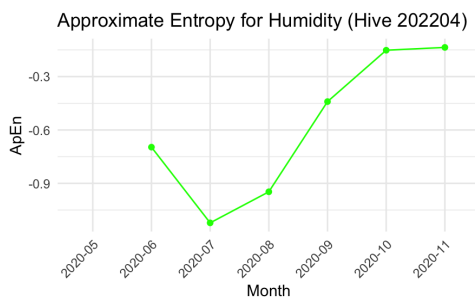


Figure 5: Approximate Entropy for Humidity

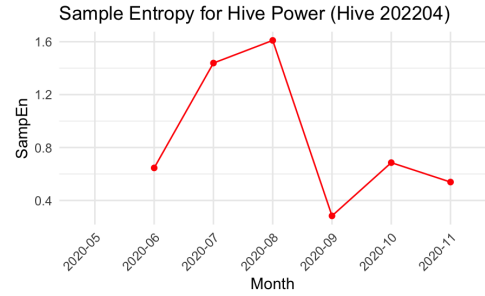


Figure 9: Sample Entropy for Hive Power

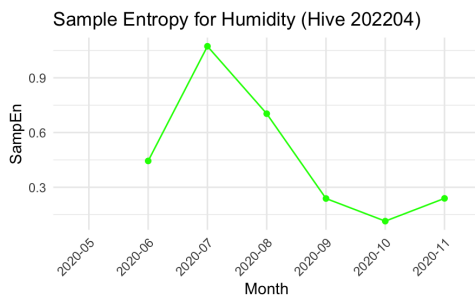


Figure 6: Sample Entropy for Humidity (Hive 202204)

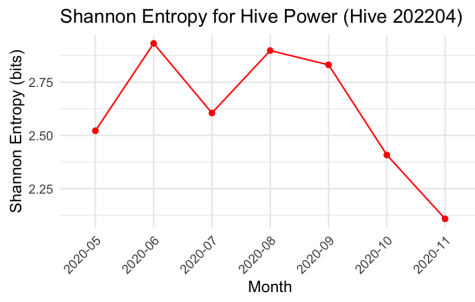


Figure 7: Shannon Entropy for Hive Power

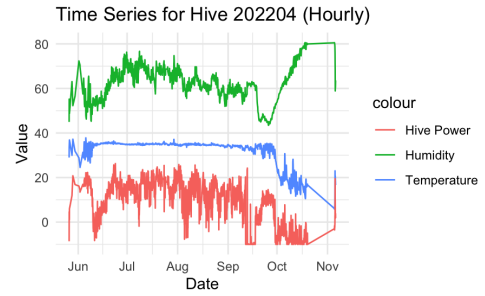


Figure 10: Time Series for Hive 202204 (Hourly)

Entropy analysis revealed distinct seasonal patterns across all three variables. For temperature, Shannon Entropy remained relatively low and stable throughout the observed period ($\tilde{2.0}$ – 2.5 bits), indicating effective thermoregulation by the colony. A slight rise in entropy during the summer months (June–August 2020) suggests minor external influences. Sample Entropy peaked at 0.74 in July and dropped to 0.29 in November, while Approximate Entropy values were negative, reflecting regularity but also potential calculation instability [3].

For humidity, Shannon Entropy peaked in October (3.17 bits), then dropped sharply in November, likely due to environmental stabilization inside winter chambers. Sample Entropy values followed a similar trend, with a summer peak (1.07 in July) and significant decline in fall. Approximate Entropy again showed negative values, with increasing irregularity observed later in the season [3].

Hive power, derived from acoustic features, exhibited the most dynamic changes. Shannon Entropy peaked at 2.93 bits

in June and declined to 2.11 bits by November, suggesting intense summer activity followed by winter quiescence. Sample Entropy confirmed these fluctuations, with high values in August (1.61) and a marked decrease in November (0.54). These trends likely reflect biologically significant events such as swarming or brood rearing during peak activity. Approximate Entropy remained negative and erratic, indicating computational limitations for this variable [3].

A time series plot of all three variables further supports these findings. Hive power displayed erratic variability during summer and stabilized toward late fall. Meanwhile, humidity remained relatively constant (50–70%), gradually increasing toward winter. Temperature followed a seasonal downward trend, dropping from $\tilde{30}^{\circ}\text{C}$ to $\tilde{20}^{\circ}\text{C}$ by November, consistent with environmental cooling [3].

Month	Temp_Sha	Humid_Sha	Power_Sha
May-20	2.52	2.52	2.52
Jun-20	1.87	2.98	2.93
Jul-20	1.63	2.76	2.61
Aug-20	2.60	2.96	2.90
Sep-20	2.38	3.09	2.83
Oct-20	2.79	3.17	2.41
Nov-20	2.49	2.20	2.11

Table 1: Shannon Entropy values for Hive 202204 (May–Nov 2020).

Month	Temp_ApE	Humid_ApE	Power_ApE
May-20	NA	NA	NA
Jun-20	-0.30	-0.70	-0.93
Jul-20	-1.14	-1.12	-1.38
Aug-20	-0.97	-0.95	-1.40
Sep-20	-0.68	-0.44	-0.77
Oct-20	-0.60	-0.15	-1.17
Nov-20	-0.09	-0.14	-0.23

Table 2: Approximate Entropy (ApEn) values for Hive 202204 (May–Nov 2020).

Month	Temp_Sam	Humid_Sam	Power_Sam
May-20	NA	NA	NA
Jun-20	0.13	0.44	0.65
Jul-20	0.74	1.07	1.44
Aug-20	0.68	0.70	1.61
Sep-20	0.26	0.24	0.28
Oct-20	0.45	0.11	0.69
Nov-20	0.29	0.24	0.54

Table 3: Sample Entropy (SampEn) values for Hive 202204.

*Note: ApEn values are omitted due to negative results, suggesting calculation issues

4 Comparison with Hive 202202 and Data Team Findings

The data team’s analysis (Page 8, Figure 6) reported hive_power’s seasonal variations across 53 hives:

summer peaks (June–August 2020) from super addition and swarming, fall fluctuations (September–October) from Varroa treatment, and winter stability (November onward) in indoor chambers [3]. They noted hive_power’s high variability, capturing colony-specific dynamics (Page 8) [3]. For hive 202204, hive_power’s Shannon Entropy (Figure 7, Page 2) peaks in June (2.93 bits), remains high in July–August (2.61–2.90), and drops to 2.11 in November, mirroring the data team’s summer activity peaks and winter stabilization [3]. SampEn (Figure 9, Page 2) peaks in August (1.61), drops to 0.54 in November, reflecting complex summer patterns (e.g., swarming, evaluations) and winter regularity [3]. The time series (Figure 10, Page 3) confirms hive_power’s erratic summer fluctuations and winter stability, consistent with interventions like super addition (June–August) and winterization (November) [3]. ApEn (Table 1) is less reliable due to negative values, possibly from implementation issues (e.g., small r in approx_entropy). Assuming hive 202202 at the Côté apiary shares identical management (e.g., super addition, Varroa treatment), its hive_power entropy would likely follow similar trends: high summer entropy (June–August) and low winter entropy (November) [3]. Without 202202’s specific data, we hypothesize consistency based on environmental and management similarities. Our entropy analysis replicates the data team’s findings, with Shannon Entropy and SampEn capturing hive_power’s seasonal dynamics more robustly than ApEn [3]. The monthly granularity provides finer insights compared to the data team’s daily averages, highlighting entropy’s sensitivity to colony activity [3, 4].

5 Transfer Entropy Analysis and Surrogate-based significance test

Month	TE_temp→power	TE_power→temp	DirIndex
06	-0.0696	0.0813	-0.151
07	-0.1193	-0.0394	-0.080
08	-0.1172	-0.0068	-0.110
09	0.1139	0.0383	+0.076
10	0.1385	0.0254	+0.113

Table 4: Transfer Entropy and Directionality Index for Temperature → Hive Power.

Month	TE_humid→power	TE_power→humid	DirIndex
06	0.1057	0.0811	+0.025
07	0.0291	-0.0562	+0.085
08	0.0141	0.1713	-0.157
09	0.0098	0.1229	-0.113
10	0.0292	0.0375	-0.008

Table 5: Transfer Entropy and Directionality Index for Humidity → Hive Power.

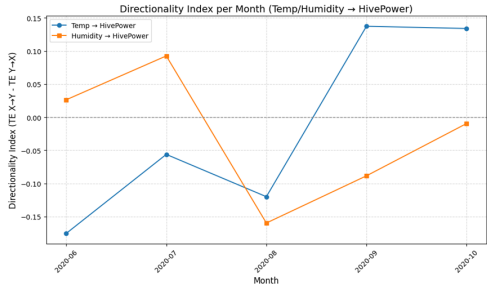


Figure 11: Directionality Index per Month(Tem/Humidity to HivePower)

Month	TE_temp→power	p-value
2020-06	-0.077698	0.88
2020-07	-0.099055	0.85
2020-08	-0.121769	0.95
2020-09	0.137959	0.10
2020-10	0.150305	0.12

Table 6: Surrogate-based significance test for Transfer Entropy (Temperature → Hive Power).

Month	TE_humid→power	p-value
2020-06	0.104871	0.09
2020-07	0.028398	0.40
2020-08	0.013782	0.51
2020-09	0.006512	0.48
2020-10	0.034606	0.40

Table 7: Surrogate-based significance test for Transfer Entropy (Humidity → Hive Power).

Although the Transfer Entropy analysis did not yield statistically significant results, visual inspection of the directionality index plot suggests possible trends in information flow between hive behavior and environmental variables. Specifically, from June to August 2020, the directionality index for temperature is negative, indicating slightly stronger information flow from hive_power to temperature. This may reflect active thermoregulatory behavior during peak colony activity. In September and October, the index reverses and turns positive, suggesting that temperature increasingly predicts hive_power, potentially signaling a shift toward passive environmental adaptation. The humidity → hive_power directionality index, on the other hand, fluctuates across months, with a pronounced dip in August, hinting at transient feedback, but lacking a consistent pattern—supporting the idea that humidity plays a relatively minor or background role in behavioral modulation.

In Transfer Entropy analysis, surrogate testing is used to determine whether the observed TE value is significantly greater than would be expected by chance. This involves randomizing the source variable (e.g., temperature or humidity) to break any temporal structure and generate a null distribution. If the actual TE exceeds most surrogate values, it suggests a meaningful directional influence rather than a spurious correlation.

As shown in the tables, none of the p-values fall below the 0.05 significance threshold. This indicates that neither temperature nor humidity exhibits statistically significant information flow to hive_power during any month. Although certain months (e.g., September and October 2020) show slightly elevated TE values, these should be interpreted cautiously as exploratory findings without statistical support.

Given the lack of statistical significance, these patterns should be interpreted as exploratory, offering a basis for future investigations using larger or higher-resolution datasets.

Although the Transfer Entropy analysis did not yield statistically significant results, the directionality indices across months revealed systematic fluctuations, particularly a reversal around the summer-to-fall transition. Since the temporal scale of information transfer may vary across conditions, relying solely on aggregate TE values could obscure meaningful dynamic patterns. Therefore, we proceeded with a Characteristic Time Scale analysis to identify the optimal lag at which temperature and humidity most strongly influence hive_power. This allows us to explore whether the timing of environmental-behavior coupling shifts across seasons—a question that remains relevant even when the overall TE magnitude lacks statistical significance.

6 Characteristic Time Scale

Month	Best Lag (hours)	Max TE
2020-06	20	0.091447
2020-07	6	0.053804
2020-08	20	0.099630
2020-09	3	0.061664

Table 8: Characteristic Time Scale for Temperature → Hive Power.

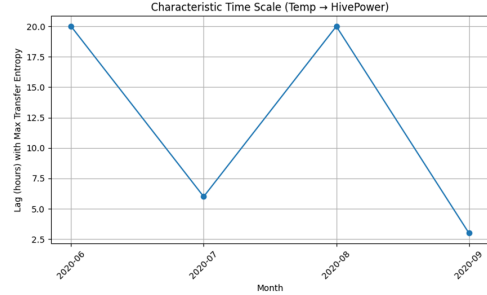


Figure 12: Characteristic Time Scale(Temp to Hivepower)

The Characteristic Time Scale analysis indicates notable month-to-month variation in the optimal lag at which temperature most strongly predicts hive_power. In June and August 2020, the highest transfer entropy occurred at a 20-hour lag, suggesting a prolonged delay in behavioral response to temperature shifts—potentially due to gradual thermoregulatory mechanisms. In contrast, the lag shortened to 6 hours in July and just 3 hours in September, implying a quicker reaction by the colony to temperature changes during these months. Notably, the sharp drop in September may signal a

behavioral adjustment as the hive transitions into fall. Overall, the time scale follows a "longer in summer, shorter in fall" pattern, consistent with the hypothesis that the rhythm of environmental-behavior coupling accelerates as seasons change.

Month	Best Lag (hours)	Max TE
2020-06	10	0.087963
2020-07	1	0.059427
2020-08	22	0.122362
2020-09	2	0.066048
2020-10	20	0.021934

Table 9: Characteristic Time Scale for Humidity → Hive Power.

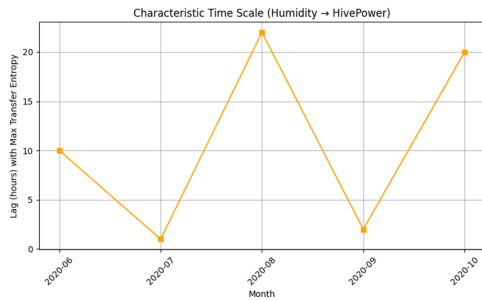


Figure 13: Characteristic Time Scale(Humidty to Hivepower)

In the analysis of characteristic time scale for Humidity → HivePower, the observed lag times varied greatly across months, suggesting an unstable or inconsistent influence of humidity on hive activity. As shown in the figure, the peak information transfer occurred at a 10-hour lag in June, dropped sharply to 1 hour in July, spiked to 22 hours in August, and again dropped to 2 hours in September before rising to 20 hours in October. These abrupt fluctuations imply that hive responses to humidity changes were neither consistent nor robust, potentially indicating that humidity is not a primary behavioral driver. Moreover, none of the transfer entropy values for these months passed the statistical significance threshold ($p > 0.05$), which supports the view that these lags reflect exploratory temporal trends rather than reliable causal dynamics. Nevertheless, the results raise interesting possibilities for further investigation, suggesting that under specific conditions, humidity may exert delayed effects on hive activity without being a consistently dominant factor.

During our initial analysis of characteristic time scales, we observed that several months exhibited peak Transfer Entropy (TE) values near the upper bound of our predefined lag window ($\text{max_lag} = 20$ hours). This raised a valid concern that our lag range might be too narrow, potentially missing stronger information flow at longer delays. To address this, we extended the lag window to 24 hours and visualized TE values across this broader range for each month.

Results showed that in June and August 2020, TE peaked near or beyond 20 hours, suggesting that meaningful interactions may exist at longer delays. These late peaks may reflect

lagged behavioral responses of the hive to humidity fluctuations, such as adjustments in internal microclimate through collective activity. In contrast, July and September exhibited TE peaks at shorter lags (1–6 hours), indicating high variability in the temporal structure of information flow across months. Although TE magnitudes varied across lags, the overall values remained low and failed to pass surrogate significance testing. Therefore, these time-scale trends should be interpreted cautiously as exploratory signals rather than definitive causal mechanisms.

7 Conclusion

Our analysis shows that entropy measures, particularly Shannon Entropy and SampEn, effectively capture seasonal changes in hive behavior. Hive power demonstrated the clearest variation, with entropy peaking in summer and declining in late fall, aligning with known colony events like swarming and winter preparation. While Approximate Entropy produced unstable results, the other metrics proved consistent. Transfer Entropy and directionality indices did not yield statistically significant patterns, though exploratory trends suggest temporal asymmetries in environmental-behavior coupling. The characteristic time scale analysis further revealed that hive responses to temperature occur over shorter lags in fall than summer, reflecting seasonal adaptation. Despite the limited statistical power, entropy-based methods showed sensitivity to subtle shifts in colony dynamics and offer promising tools for non-invasive behavioral monitoring. Future work should validate these findings across more hives and longer periods, potentially integrating higher-resolution data or experimental interventions.

References

- [1] Klein, A.-M., et al. (2007). Importance of pollinators in changing landscapes for world crops. *Proceedings of the Royal Society B: Biological Sciences*, 274, 303–313.
- [2] Abdollahi, M., Giovenazzo, P., & Falk, T. H. (2022). Automated beehive acoustics monitoring: A comprehensive review of the literature and recommendations for future work. *Applied Sciences*, 12, 3920.
- [3] Zhu, Y., Abdollahi, M., Maucourt, S., Coallier, N., Guimarães, H. R., Giovenazzo, P., & Falk, T. H. (2023). MSPB: A longitudinal multi-sensor dataset with phenotypic trait measurements from honey bees (*Apis mellifera L.*). *arXiv preprint*, arXiv:2311.10876. Available at <https://arxiv.org/pdf/2311.10876.pdf>.
- [4] Richman, J. S., & Moorman, J. R. (2000). Physiological time-series analysis using approximate entropy and sample entropy. *American Journal of Physiology-Heart and Circulatory Physiology*, 278(6), H2039-H2049.